M 2021

U.PORTO
FEUP FACULDADE DE ENGENHARIA
UNIVERSIDADE DO PORTO

A LOW FOOTPRINT OZONE MIXER BASED ON THE NETMIX TECHNOLOGY: CFD MODELLING AND EXPERIMENTAL VALIDATION

PAULO HENRIQUE MARROCOS DE OLIVEIRA

MASTER'S DISSERTATION PRESENTED
TO THE FACULTY OF ENGINEERING OF THE UNIVERSITY OF PORTO IN
CHEMICAL ENGINEERING

Master in Chemical Engineering

A low footprint ozone mixer based on the NETmix technology: CFD modelling and experimental validation

Master dissertation

of

Paulo Henrique Marrocos de Oliveira

Developed within the course of dissertation

held in

Associate Laboratory LSRE-LCM

SRE CM ASSOCIATE LABORATORY
LABORATORY OF SEPARATION AND REACTION ENGINEERING
LABORATORY OF CATALYSIS AND MATERIALS

Supervisor: **Dr. Vítor Jorge Pais Vilar**

Co-Supervisor: **Dr. Ricardo J. N. Santos**

U.PORTO
FEUP FACULDADE DE ENGENHARIA
UNIVERSIDADE DO PORTO

DEPARTAMENTO DE
ENGENHARIA QUÍMICA

July 2021

“And so, does the destination matter? Or is it the path we take?

I declare that no accomplishment has substance nearly as great as the road used to achieve it. We are not creatures of destinations. It is the journey that shapes us. Our callused feet, our backs strong from carrying the weight of our travels, our eyes open with the fresh delight of experiences lived.”

Brandon Sanderson, *The Way of Kings*

Agradecimentos

Em sua obra “Meditações”, Marco Aurélio, o imperador romano de maior sucesso e exemplo de filósofo estoico, dedica o primeiro capítulo para estender sua gratidão aos eventos e às pessoas dos quais lições foram extraídas, adicionando-as à sua composição de carácter. Eu, como um admirador do estoicismo, aqui buscarei seguir seus passos.

Aos meus orientadores; Doutor Vítor Vilar e Doutor Ricardo Santos, pela oportunidade, orientação, disponibilidade, aprendizagem e paciência. Isabel, quem, apesar de não poder oficialmente compor a equipa de orientadores, escolheu continuar a me ensinar de bom grado, com qualidade e tranquilidade. Yaidelin e Mateus, os quais me deram suporte nos ensaios experimentas deste trabalho.

À minha família; minha querida mãe, quem construiu comigo as bases da minha identidade, da minha índole, e do meu julgamento, quem, como alavanca, me elevou como ser humano, para que, posteriormente, me fornecesse ferramentas com as quais eu pudesse construir a mim mesmo, entretanto, quem está sempre presente para qualquer necessidade. Meu pai e meu tio, os quais me aconselharam, me guiaram e me auxiliaram.

Aos meus amigos; Débora, quem, além de me acolher no seu espaço, foi a ponte que me permitiu trespassar um oceano. Luísa, Lívia, Jorge e João, os quais ajudaram a tornar familiares terras uma vez desconhecidas. Eduarda, cuja confiança enobreceu minha compreensão de amizade. Bianca, Rharyne e Débora, as quais foram abrigo em tempos de tempestade, e reforçaram meu sentido de integridade. Rebeca e Bruno, cujas lições foram mais valiosas que as minhas de matemática e física. Rita, quem, às vezes, levou meu sorriso, meu assunto.

Diferente do Marco Aurélio, o qual não tinha limite de páginas na sua obra, me foi fornecida apenas esta página no meu trabalho para o capítulo de agradecimentos. Por isso, estendo minha gratidão àqueles que não encontraram aqui seus nomes, contudo por mim não são esquecidos.

Este trabalho foi suportado por: Financiamento Base - UIDB/50020/2020 do Laboratório Associado LSRE-LCM e projeto PTDC/EAM-AMB/4702/2020 (OZONE4WATER) - financiado por fundos nacionais através da FCT/MCTES (PIDDAC).

O Doutor Vítor Vilar e o Doutor Ricardo Santos, orientadores desta dissertação, são membros integrados do Laboratório Associado LSRE-LCM com financiamentos Base-UIDB/50020/2020 e Programático-UIDP/50020/2020 do LSRE-LCM, financiado por fundos nacionais através da FCT/MCTES (PIDDAC).

Abstract

Among the oxidation technologies, ozonation presents itself as a suitable method for both disinfection and oxidation due to its high efficiency to kill microorganisms, as well as its high redox potential to oxidize organic and inorganic pollutants. However, the gas/liquid mass transfer is a rate-limiting step in ozonation. As the NETmix is a novel static mixer technology with a high mixing efficiency, it shows itself as an adequate alternative to enhance the ozone mass transfer from the gas phase to the liquid phase to 100% or very close to it. Hence, to determine the best conditions for the dissolution of the ozone in the liquid as well as to understand the main flow properties intrinsic to this multiphase flow inside the NETmix, this work aims to develop a Computational Fluid Dynamics (CFD) model that describes the flow of ozone and water in the static mixer, and validate it experimentally.

The proposed 2D CFD model, based on the Volume of Fluid approach, was implemented in two geometries, the NETmix Unit Block (NUB), and a proposed geometry which considers the shape of the entrance at which each phase is injected in the NETmix. The results obtained from the CFD simulations were compared with experimental data, which consisted of images of the multiphase flow at the same conditions of the simulations.

To test and validate the model, two flow parameters were considered: the direction of the flow - upwards and downwards -, and the ratio of gas and liquid volumetric flowrates. The comparison of both numerical and experimental results showed that the model makes an accurate description of the multiphase flow inside the NETmix, capable of predicting the behaviour, shape and size of gas bubbles as they move throughout the static mixer, as well as simulating the phenomena related to all tested ratios and flow directions. Additionally, a combined analysis of the simulations and the experiments led to the conclusion that the downwards direction is the most favorable regarding the gas transfer to the liquid phase. When the two directions were compared under the same gas and liquid flowrate values, the downwards direction provided at least twice the gas passage time in relation to the upwards direction, and a higher concentration of gas inside the NETmix. It was also proven that the entrance shape has no influence on the formation of bubble shape and size if the gas phase occupies the entirety of the inlet channel connected to the entrance chamber of the NETmix, whereby, in this case, the decisive factor of bubble formation is the dimension of such channel.

Keywords: ozone mass transfer, NETmix, computational fluid dynamics (CFD), experimental validation, multiphase flow.

Resumo

Entre as tecnologias de oxidação, a ozonização é um método adequado para desinfeção e oxidação dada a sua alta eficiência para inativar microrganismos, bem como o seu alto valor de potencial redox para oxidar poluentes orgânicos e inorgânicos. Contudo, a transferência de massa gás/líquido é um passo limitante na ozonização. Como o NETmix é uma nova tecnologia de misturadores estáticos com uma alta eficiência de mistura, este apresenta-se como uma alternativa adequada para intensificar a transferência de massa do ozono da fase gasosa para a fase líquida para 100% ou próximo deste valor. Deste modo, a fim de determinar as melhores condições para a dissolução do ozono no líquido, assim como compreender as principais propriedades intrínsecas a este escoamento multifásico no interior do NETmix, este trabalho visa desenvolver um modelo em Dinâmica de Fluidos Computacionais (CFD) que descreva o escoamento de ozono e água no misturador estático, e validá-lo experimentalmente.

O modelo 2D de CFD proposto, baseado na abordagem Volume de Fluido, foi implementado em duas geometrias, o NETmix Unit Block (NUB) e uma nova geometria que considera o formato da entrada na qual cada fase é injetada no NETmix. Os resultados obtidos pelas simulações CFD foram comparadas com dados experimentais, os quais consistiram em imagens do escoamento multifásico nas mesmas condições das simulações.

A fim de testar e validar o modelo, dois parâmetros foram considerados: a direção do escoamento - ascendente e descendente -, e a razão de caudais volumétricos do gás e do líquido. A comparação entre resultados numéricos e experimentais mostrou que o modelo descreve com precisão o escoamento multifásico no interior do NETmix, sendo capaz de prever o comportamento, o formato e o tamanho de bolhas de gás enquanto elas se movem pelo misturador estático, além de simular o fenómeno relacionado a todos os parâmetros testados. Ademais, com uma análise combinada das simulações e dos ensaios experimentais, concluiu-se que a direção descendente é a mais favorável à transferência do gás para a fase líquida. Quando as duas direções foram comparadas sob os mesmos valores de caudais de gás e líquido, a direção descendente forneceu pelo menos o dobro de tempo de passagem do gás em relação à direção ascendente, e uma maior concentração de gás no interior do NETmix. Também foi provado que o formato da entrada não tem influência na produção da forma e do tamanho da bolha se a fase gasosa ocupar inteiramente o canal de entrada conectado à câmara de entrada do NETmix, em que, neste caso, o fator decisivo para a formação das bolhas é a dimensão de tal canal.
Palavras-chave: transferência de massa de ozono, NETmix, dinâmica de fluidos computacionais (CFD), validação experimental, escoamento multifásico

Declaration

I hereby declare, under word of honor, that this work is original and that all non-original contributions is indicated and due reference is given to the author and source

Porto, 5 of July of 2021

Paulo Henrique Marrocos de Oliveira

Index

1 Introduction 1

1.1 Framing and presentation of the work 1

1.2 Contributions of the author to the work 2

1.3 Organization of the dissertation 2

2 Context and State of the art 4

2.1 Ozone 4

2.1.1 Applications of ozone 6

2.1.2 Limitations 7

2.2 Ozone dissolution equipment 7

2.2.1 Fine bubble diffuser 8

2.2.2 Packed column 8

2.2.3 Sparged or self-inducing impellers 9

2.2.4 Injectors and static mixers 9

2.3 NETmix 11

2.4 Computational fluid dynamics and its applications 13

3 Materials and Methods 15

3.1 Volume of Fluid model 16

3.2 Geometry and mesh 17

3.3 Boundary and initial conditions 18

3.4 Solution methods 20

4 Results and discussion 22

4.1 Preliminary study of flow properties 22

4.2 Analysis of flow properties and simulation validation 29

4.2.1 Condition A 29

4.2.2 Condition B 32

4.2.3 Condition C 35

4.2.4 Condition D 37

4.3 Analysis of entrance shape influence on the bubble formation 39

5 Conclusion 43

6 Assessment of the work done 45

6.1 Objectives achieved 45

6.2 Final assessment 45

7 References 46

Appendix A – Experimental setup 51

Appendix B – Contact angle measurement 53

Appendix C – Extention of Condition B results 54

Appendix D – Rigorous calculation of the increase in gas passage time from upwards flow to downwards flow 56

List of Figures

Figure 1 - Simplified cycle presenting the main species involved in the decomposition of ozone in pure water at pH 7 (adapted from [14]). 5
Figure 2 -A) Ozone bubble fine diffuser contactor; B) Packed column; C) Baffled sparged impellers; D) Sidestream configuration using a venturi injector; E) Ozone static mixer from Komax Systems, inc. (adapted from [7,25,29,33,34]) 11
Figure 3 -A) Three-dimensional representation of a NETmix in a plate, in which the unit cells are composed of a cylindrical chamber, and the channels are rectangular prisms; B) Example of a unit cell in which the chamber is a cylinder, and the channel, a rectangular prism; C) Example of a unit cell in which the chamber is a sphere, and the channel is a cylinder. 12
Figure 4 – Geometry, characteristic dimensions and boundary conditions for the A) NETmix Unit Block used in this work; B) Half Network Geometry. 18
Figure 5 - Pattern of injection of both phases inside the NETmix for all experiments. 23
Figure 6 – Flow images for the upflow direction, for the ratio of gas volumetric flowrate and liquid volumetric flowrate (GL) of values 0.1, 0.25 and 0.5. 24
Figure 7 - Flow images for the upflow direction, for the ratio of gas volumetric flowrate and liquid volumetric flowrate (GL) of values 1, 2 and 4. 25
Figure 8 - Flow images for the downflow direction, for the ratio of gas volumetric flowrate and liquid volumetric flowrate (GL) of values 0.1, 0.25 and 0.5. 26
Figure 9 – Flow images for the downflow direction, for the ratio of gas volumetric flowrate and liquid volumetric flowrate (GL) of values 1, 2 and 4. 27
Figure 10 - A) Results, at different indicated times, of the simulation performed at condition A. The gas phase is indicated by the red colour, whereas the blue colour is the liquid phase; B) Two photographs taken from the experiment performed at condition A. 30
Figure 11 – Velocity contour displaying the main trajectory taken by the liquid, highlighted in green, and the region where the gas bubbles can be trapped, highlighted by the red circle. 31
Figure 12 - Evolution of volume fraction of gas and liquid phases for the condition A as a function of time divided by the passage time. 32
Figure 13 - A) Results, at different indicated times, of the simulation performed at condition B. The gas phase is indicated by the red colour, whereas the blue colour is the liquid phase; B) Two photographs taken from the experiment performed at condition B. 33
Figure 14 - Evolution of volume fraction of gas and liquid phases for the condition B as a function of time divided by the passage time. 34
Figure 15 – A) Results, at different indicated times, of the simulation performed at condition C. The gas phase is indicated by the red colour, whereas the blue colour is the liquid phase; B) Two photographs taken from the experiment performed at condition C. 36
Figure 16 - Evolution of volume fraction of gas and liquid phases for the condition C as a function of time divided by the passage time. 36

Figure 17 - A) Results, at different indicated times, of the simulation performed at condition D. The gas phase is indicated by the red colour, whereas the blue colour is the liquid phase; B) Two photographs taken from the experiment performed at condition D. *37*
Figure 18 - Evolution of volume fraction of gas and liquid phases for the condition D as a function of time divided by the passage time. *38*
Figure 19 - Comparison of the behaviour of the phases at the inlets between the HNG without the entrance chamber, and the NUB geometry. The picture from the HNG comes from the Figure 20, at time $t = 0.25\tau$*; whereas the NUB picture, from Figure 10, at time* $t = 2\tau$*.* *41*
Figure 20 - A) Results, at four different indicated times, of the simulation performed with the HNG. The gas phase is indicated by the red colour, whereas the blue colour is the liquid phase; B) Two photographs taken from the experiment performed at conditions equivalent of the simulation done with the HNG. *42*
Figure 21 - Diagram with the experimental setup used in this work. *51*
Figure 22 - The NETmix unit, the mass flow controller and the distributors which compose the experimental setup utilised in this work. *52*
Figure 23 - Picture of each of the four contact angle measurements at 10 s after the drop of water droplet on the surface of the stainless steel 316 slab, containing measurements performed by the software. *53*
Figure 24 - A) Results, at different indicated times, of the simulation performed at condition B, extended to 5τ*. The gas phase is indicated by the red colour, whereas the blue colour is the liquid phase; B) Two photographs taken from the experiment performed at condition B.* *55*
Figure 25 - Evolution of volume fraction of gas and liquid phases for the condition B, extended to 5τ*, as a function of time divided by the passage time.* *55*

List of Tables

Table 1 - Properties of ozone [13,15]. 4
Table 2 – Henry's law constant for given temperatures, in which it is compared the species ozone, in conditions realistic to its applications, and oxygen (adapted from [13]). 6
Table 3 - Range of values of volumetric mass transfer coefficients for the equipment most used in the dissolution of ozone in water/wastewater plants (adapted from [31,32]). 10
Table 4 - Chosen spatial discretisation for the indicated quantities. 20
Table 5 -Values of ratio of gas volumetric flowrate and liquid volumetric flowrate tested in the experiment, along with corresponding Reynolds number for each phase. 22
Table 6 – Selected experiments to be simulated, for which a name is given to the corresponding parameters of the experiment. 29
Table 7 - Fluid properties used in the simulations of conditions A to D. The decimal places were kept unchanged to indicate the precision used in the simulations. 29
Table 8 - Fluid properties used in the simulation with the HNG. The decimal places were kept unchanged to indicate the precision used in the simulations. 39
Table 9 - Results obtained for the steady state average value of the overall gas volume fraction for each condition tested in this work. 57
Table 10 - Results of the increase in gas passage time when the flow directions is changed from upwards to downwards, for each ratio value tested. 57

Notation and Glossary

A	Cross sectional area of the NETmix channel	m^2
$A_{geometry}$	Area of the used geometry	m^2
Co	Courant number	
d	Width of a NETmix channel	m
D_1	Diameter of a NETmix chamber	m
D_2	Diameter of a smaller NETmix channel	m
D_h	Hydraulic diameter	m
D_{in}	Diameter of a NETmix inlet	m
$\vec{F}$	External forces source term	$Pa \cdot m^{-1}$
F_{vol}	Volume force	$Pa \cdot m^{-1}$
$\vec{g}$	Gravitational acceleration vector	$m \cdot s^{-2}$
$\frac{G}{L}$	Ratio of gas volumetric flowrate and liquid volumetric flowrate	
H	Henry's law constant	$mol\ m^{-3}$ Pa^{-1}
$k_L a$	Volumetric mass transfer coefficient	s^{-1}
L	Length of a NETmix channel	m
$\dot{m}_i$	Mass flowrate of phase i	$kg \cdot s^{-1}$
$\hat{n}$	Unit vector normal to surface of the interface	
$\hat{n}_w$	Unit vector normal to the wall	
$N_{in,i}$	Number of inlets in which the phase i enters	
P	Wet perimeter	m
pH	Potential of hydrogen	
Q_i	Volumetric flowrate of phase i	$m^3 \cdot s^{-1}$
$\mathrm{Re_i}$	Reynolds number associated with the fluid i	
t	Time	s
$\hat{t}_w$	Unit vector tangential to the wall	
V_{NETmix}	Volume of the NETmix	m^3
$\vec{v}$	Velocity vector field	$m \cdot s^{-1}$
v_{Max}	Velocity proportional to the maximum fluid velocity	$m \cdot s^{-1}$
$v_{in,i}$	Velocity of the fluid i calculated at the first contacting channel	$m \cdot s^{-1}$

Greek Letters

α_G	Volume fraction of the gas phase	
α_L	Volume fraction of the liquid phase	
Δt	Time step size	s
Δx	Mesh element size	m
θ	Contact angle	º
κ_G	Curvature associated with the gas phase	m^{-1}
κ_L	Curvature associated with the liquid phase	m^{-1}
μ	Volume-fraction-averaged dynamic viscosity	Pa·s
μ_G	Gas phase dynamic viscosity	Pa·s
μ_L	Liquid phase dynamic viscosity	Pa·s
ρ	Volume-fraction-averaged mixture density	$kg \cdot m^{-3}$
ρ_G	Gas phase density	$kg \cdot m^{-3}$
ρ_L	Liquid phase density	$kg \cdot m^{-3}$
σ	Surface tension	$N \cdot m^{-1}$
τ	Passage time	s

Indexes

G	Gas phase
h	Hydraulic
i	Index associated to either G or L (Gas or Liquid, respectively)
j	Index associated to either U or D (Upwards or Downwards, respectively)
in,i	Phase i at the inlet
L	Liquid phase
q	Generic phase q
vol	Volume

List of Acronyms

CFD	Computational Fluid Dynamics
CFL	Courant-Friedrichs-Lewy
CSF	Continuum Surface Force
HNG	Half Network Geometry
MUSCL	Monotone Upstream-Centered Schemes for Conservation Laws
NUB	NETmix Unit Block
PRESTO!	Pressure Staggering Option
SIMPLEC	Semi-Implicit Method for Pressure Linked Equations-Consistent
VOF	Volume of Fluid

1 Introduction

1.1 Framing and presentation of the work

Ozonation is an advanced oxidation technology suitable for disinfection, as well as degradation of inorganic and organic substances. It has a proven high efficiency and wide adaptability to kill microorganisms due to its high redox potential to oxidize compounds. The instability of ozone dictates the need for on-site generation, usually by applying the Corona process to pure oxygen streams [1]. One major obstacle to a general wider use of ozone technology is its high associated ozone generation costs stemming from the fact that only a small fraction of the initial high-purity oxygen feed (10-15 wt-%) is able to be converted into ozone. The specific power rises from 7.2 to 12.3 kW/kg O_3, when the O_3 concentration is increased from 6% to 12%, which is an increase of 71% [2]. The supply of pure O_2 is also an important cost factor. Traditionally, O_3 is dispersed by bubbling a gas mixture of typically 6% to 12% (wt) O_3 into the water via bubble diffusers, injectors, or static mixers [3]. While the principles of direct gas-liquid mass transfer of O_3 into the aqueous phase are well understood, bubbling methods bear a number of disadvantages, such as locally inaccurate O_3 dosages due to short-circuiting, low ozone mass transfer rates from gas to liquid phase, foam formation in treatment reactors, bubble coalescence and uneconomic off-gas recovery (mainly O_2) [2].

Many mixing equipment were developed to transfer the ozone into the water, among which the fine bubble diffuser contactor is the most common, due to its simplicity, robustness and requiring no additional energy than the initial gas compression [4]. In this system, the ozone is injected through a porous stone diffuser below the contactor, creating small bubbles by which an ozone rich liquid is created. Thereafter, this ozone rich liquid is used inside the same chamber to perform the reactions of disinfection and oxidation. An alternative is to use a sidestream injection system, whereby there is a physical separation of the dissolution and the reaction processes. Sidestream injection involves splitting off a portion of the main water flow into a side stream, then, O_3 is injected into this stream by an equipment such as a venturi injector, or, more efficiently, a static mixer, and the concentrated O_3 side stream is mixed back into the main flow [5].

A static mixer consists of a series of fixed elements responsible for modifying the flow paths of the fluid. Besides the enhanced mixing efficiency, this system benefits from low equipment, energy, and operating costs, as well as small space requirements [6,7]. A novelty in the technology of static mixers is the NETmix [8], which is a network composed of identical unit cells, whereby each chamber is interconnected by two inlet and two

outlet half channels. In addition to the benefits intrinsic to static mixers, the NETmix offers other characteristics and advantages, such as the ability to control the degree of mixing, as well as the property of operating at lower pressure drops [9,10].

One of the tools used in the investigations associated with the NETmix was the Computational Fluid Dynamics (CFD), which is a set of numerical techniques utilised to solve a mathematical model developed to describe a phenomenon based on the dynamics of the fluid [11]. Through the resolution of the conservation and transfer equations, CFD simulations provide a complete picture of the flow, enabling an alternative way to both understand the phenomena inside the NETmix, and optimize its configurations so that efficient operational conditions are achieved. CFD has had success in representing the single phase flow in the NETmix [6,10], with recent studies showing its potential to describe a gas-liquid flow inside the static mixer [12].

Therefore, the objective of this work is to develop a multiphase model using the CFD tool, capable of describing the flow of ozone and water inside a NETmix unit, enabling the evaluation of the mixer geometry and flow parameters on the mass transfer of gas into liquid. This model will be a useful tool to determine the best conditions to introduce the NETmix as a novel ozone mixing technology for water and wastewater treatment. Furthermore, this work aims to validate the model through a comparison between numerical and experimental data, as well as to use both results to comprehend the main flow properties intrinsic to this two-phase flow.

1.2 Contributions of the author to the work

The author has developed a geometry to simulate a NETmix unit, physically available in the Associate Laboratory LSRE-LCM/FEUP, with which the author has constructed an adequate mesh where the calculations were performed. The proposed CFD model was created through research performed by the author, as well as discussions with the supervisors. Moreover, the experimental tests were done in the lab-scale facility with the collaboration of the PhD student Mateus Pituco.

1.3 Organization of the dissertation

This work is divided into six chapters hereinafter described:

Chapter 1 introduces the reader into the motivation of this work and the concepts to be treated, which are further developed in Chapter 2. In the second chapter, Section 2.1 explores the ozone, its properties and characteristics, as well as applications and limitations of the ozonation; Section 2.2 describes briefly the most common equipment in solubilizing ozone into water; Section 2.3 is dedicated to the NETmix technology,

explaining its concept, its characteristics, and exposing some previous works and applications with which it is associated; Section 2.4 is a brief explanation of the CFD tool, and a highlight of some of its applications. Chapter 3 explains the equations and models used in this work, it presents the geometries used to represent a NETmix unit, the meshes constructed for the simulations, and the criteria for the solution of the proposed model: boundary and initial conditions, as well as the method of solution of the equations. The results obtained in this work are presented and discussed in Chapter 4, thereafter Chapter 5 summarizes all conclusions made. Lastly, in Chapter 6, the achieved objectives and limitations of the work are discussed, and future works are proposed.

2 Context and State of the art

2.1 Ozone

In 1785, Martinus Van Marum identified the ozone by its characteristic odour, without recognizing it as a new substance. It was only in 1840 that Schönbein reported this odour as a new molecule which he called "ozone", derived from the Greek word *ozein*, translating into "to smell". 27 years later, in 1867, Schönbein himself confirmed the ozone structure as a triatomic oxygen molecule [13].

Along with its characteristic odour, ozone has the property of being a powerful oxidant and disinfectant, with a high value of redox potential that is reported to be one of the highest amongst the common oxidants [14]. Hence, it should, theoretically, be able to fully oxidize inorganic substances, as well as transform all organic ones into carbon dioxide, water and mineral acids.

However, the oxidation provided by the ozone is selective in its nature, in which it attacks preferably multiple bonds, to the detriment of simple bonds, and aromatic substances. Additionally, the oxidation of some organic substances is slow, leading to incomplete oxidation of these molecules, resulting into a low mineralization efficiency, i.e., a low percentage of compounds that were transformed into carbon dioxide, mineral acids and water [14,15]. Furthermore, ozone is an unstable gas, decaying rapidly and in different manners, depending on the environment in which it is. This decay is measured by the half-life of the substance, the time at the end of which the amount of the compound is reduced to half of its initial quantity. When dissolved in water, ozone half-life varies between a few seconds to a maximum of 20 minutes, dependent on the condition of the water, such as pH, temperature, and total organic carbon [13]. Other additional properties of ozone are shown in Table 1.

Table 1 - Properties of ozone [13,15].

Property	Value
Molecular Weight / $g \cdot mol^{-1}$	48.0
Boiling temperature at 1 atm / °C	-112
Density at 20 C and 1 atm / $kg \cdot m^{-3}$	2.0
Heat of formation at 1 atm, 25 °C and pH=0 / $kJ \cdot mol^{-1}$	141.7
Redox potential / V	2.07

The low values of half-life for the ozone in water are a consequence of its decomposition into various species: Figure 1 shows a cycle of ozone decomposition initiated by ions hydroxide, OH^-, when in pure water at pH 7. Though the simplified diagram presents only the main species, it is possible to illustrate the complexity of ozone decomposition in water: detailed information can be found in literature [4,15,16]. This instability property of ozone raises the possibility of an additional way of oxidation: the indirect oxidation. While the direct oxidation is the degradation by the ozone molecules themselves, the indirect oxidation is the degradation through the hydroxyl radical, $OH^{\bullet}$, produced by the decomposition of ozone. The hydroxyl radicals, unlike ozone, are unselective in its oxidative process, in addition to having a redox potential even higher than the one from ozone, 2.80 V. These properties rend it an important oxidant species [17,18].

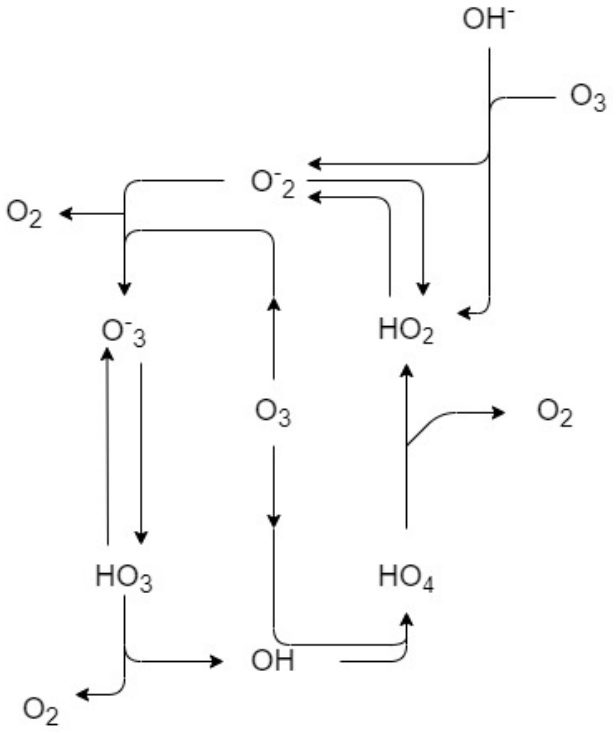

Figure 1 - Simplified cycle presenting the main species involved in the decomposition of ozone in pure water at pH 7 (adapted from [14]*).*

The solubility of ozone in water can be estimated by Henry's law, which states that, for an invariable temperature, the quantity of gas dissolved in the liquid, x, is directly proportional to the partial pressure of the gas in equilibrium with the liquid, y. Hence, the law can be translated into Equation 1:

$$y = H\,x \tag{1}$$

In which H is the Henry's law constant. Though the law has some limitations, as it can be seen in [19] for a more detailed explanation, it provides a good estimate of the solubility of ozone in water through its constant: the lower the Henry's constant is, the more soluble is the gas. As a consequence of the definition of the law, H varies with temperature and the species themselves. Table 2 shows values of the constant for ozone, and oxygen for comparison, in different conditions, for given temperatures. It can be seen that ozone is more soluble in water than oxygen: at 20 °C, ozone is roughly 11.5 times more soluble than oxygen. However, during its most common applications, ozone in the gas phase is usually in low partial pressures when in contact with the liquid, hence hardly a concentration in water of more than 100 $mg \cdot L^{-1}$ is reached [13].

Table 2 – Henry's law constant for given temperatures, in which it is compared the species ozone, in conditions realistic to its applications, and oxygen (adapted from [13]*).*

Species	**Temperature** / °C	**Henry's law constant** / $mg_{gas\ in\ gas\ phase} \cdot L_{liquid\ phase} \cdot mg^{-1}_{gas\ in\ liquid\ phase} \cdot L^{-1}_{carrier\ gas}$
Ozone 10 wt% in oxygen	0	1.7
	10	1.9
	20	2.6
	30	3.8
Oxygen 100%	0	20.4
	10	25.5
	20	29.9
	30	34.2

2.1.1 Applications of ozone

Ozone is used in various domains, ranging from food processing, medical, dental, pharmaceutical utilizations, and mainly for water treatment [20]. The amplitude of its usage lies in its properties described in the previous section: however, as the focus of this work is its application in water treatment, the two main manners of utilization of ozone in this domain will be hereinafter explored.

Due to its high redox potential, as well as great reactivity, ozone can be utilised to destroy microorganisms with high efficiency, wide adaptability and cause low impacts in the environment [21]. As such, ozone was firstly applied for drinking water disinfection. The year 1906 represented its first implementation in a water treatment plant in Nice, France. Thereafter, its usage as disinfectant for water treatment has been rising: in 1940, 119 water treatment plants utilised ozone, and, in 1972, this number had grown to at least 1039 [15].

Moreover, the properties of ozone rend it a good candidate for an oxidant. Oxidation of inorganic substances such as iron, manganese, cyanide, nitrite and hydrogen sulfide; as well as organic substances which cause odour and undesirable tastes, represents a secondary application of this gas in water treatment [5]. In drinking water treatment plants, it can be used as pre-oxidation, main oxidation and final disinfection [22].

2.1.2 Limitations

As ozone is unstable, it cannot be stored, and, as such, it must be produced *in situ*. Usually, water treatment plants use ozone generators operating through Corona discharge, which consume energy in a range of 8 to 27 kWh for each kg of ozone produced, excluding any preparation of the input gas, which can be either air or an oxygen rich gas. This high energy consumption is associated with an efficiency of only 10% of the input energy being directly used into the production of ozone: the majority of the energy is used to produce heat, light and sound [22,23]. Hence, producing ozone can be expensive, and energy inefficient.

Furthermore, the ozone generator produces typically a gas mixture with only 8 wt% to 12 wt% of ozone, when using an oxygen rich feed, and less when using air [5], which leads to a low solubility of ozone in water, as it is predicted by the Henry's law. As a consequence, usually ozone has a low mass transfer rate from the gas to the liquid phase. This results in high ozone supply demands, long contacting times between the liquid and gas phases, and equipment of considerable sizes in order to achieve the necessary concentration of ozone in the water [2,23]. As such, several studies have been done to investigate smaller equipment capable of providing higher mass transfer rates, as it will be discussed in the following section.

2.2 Ozone dissolution equipment

As ozonation occurs in the liquid phase, the ozone must be transferred from the gas phase into the liquid phase. This mass transfer is influenced by the type of equipment utilised to provide the mixing between phases, as well as other factors, such as the ozone concentration in the gas phase, the concentration of gas inside the mixing zone, the gas passage time, the ratio of gas to water, the diameter of the gas bubble, the type of reaction, and the operating conditions [4,13]. The efficiency of the gas dissolution using different equipment can be measured and compared through the volumetric mass transfer coefficient, frequently known as $k_L a$, to which the equipment is associated. The higher the coefficient, the higher is the transfer rate, for equal conditions of temperature, pressure, pH and concentration in the gas phase: consequently, the higher the efficiency [24].

Hereinafter, it will be discussed the most common mixing equipment systems for ozone applications in water treatment, and, at the end of the section, Table 3 will show a range of typical values of the volumetric mass transfer coefficients for the equipment discussed in this work.

2.2.1 Fine bubble diffuser

The fine bubble diffuser contactor is the technology most used in water treatment applications due to its simplicity, robustness, and requiring no more energy than the necessary for the initial gas compression. It consists of a series of chambers, each separated by walls called baffles, in which it both dissolves ozone into the water and provides space for the reaction of disinfection and/or oxidation. The gas injection is made through a porous stone diffuser below the contactor that creates small bubbles, as it can be seen in Figure 2A. The quantity of chambers by which it is constituted can vary depending on the application and the necessity, but it is frequent to find plants using contactors with two or three chambers [4].

This equipment is of easy maintenance, as it has no moving parts, in addition to providing an efficient ozone transfer into the liquid phase. Values ranging from 85% to 95% of the input ozone is solubilized, in which the lower value comes from gas streams with low ozone concentrations, such as 1 wt% to 2 wt%; and the higher values, from high ozone concentrations, 8 wt% to 10 wt%. However, to achieve this efficiency, it must usually be constituted of deep chambers, from 6.0 to 7.3 m, resulting in a bulky equipment [4,5]. The range of values of volumetric mass transfer coefficient shown in Table 3 is wide due to the many possibilities of arrangement, as well as the various types of diffusers and their characteristics.

2.2.2 Packed column

The gas-liquid contact provided by a packed column is continuous, in which the counter current configuration is most usual, whereby the liquid flows downwards over the packing surface, and the gas flows upwards, as it is shown in Figure 2B. The packing can be random, such as rings and saddles, which are arranged randomly inside the column; or structured, which is arranged regularly in order to provide high surface area with a high void fraction [25]. These different possibilities are associated with the range of values of volumetric mass transfer coefficient shown in Table 3.

In a water treatment plant, the packed column has been used in one of two possibilities. On the one hand, the ozone can be diffused into the water before entering the column, as such, the equipment would be used as a reactor to disinfect and/or oxide; on the other hand, the gas phase can be injected directly into the column, so that the equipment is

both a mixer of the two phases, and a reactor. The main advantage of the packed column lies in not requiring moving parts, leading to minimal mechanical maintenance. However, this equipment is not as common as the others described in this section, for the application in water treatment plants [4].

2.2.3 Sparged or self-inducing impellers

In this system, a vessel contains the liquid, inside which the gas is sparged underneath an impeller: a series of blades attached to a rotating shaft in order to create a radial flow of the fluid [26]. Consequently, the gas is dispersed into fine bubbles, raising the contact surface area of gas and liquid. Alternatively, the agitated tank can use the rotation of the impeller to create low pressure regions on the blade surfaces capable of inducing gas from the headspace into the liquid phase: an approach called the self-inducing impellers, which have the advantage of reducing gas compressing costs [27].

In the two systems, baffles are used to further improve the mixing [28]: Figure 2C shows a baffled sparged impeller. Although a high efficiency can be achieved with both systems without the need of deep vessels, an external energy source is required to power the impeller, representing an additional operating cost in order to dissolve ozone into the water [29]. Different parameters, such as the quantity of baffles and the power used, generate the range of values of volumetric mass transfer coefficient presented in Table 3: only baffled systems are shown, as there are higher values associated with them, when compared to the unbaffled ones.

2.2.4 Injectors and static mixers

A viable alternative to fine bubble diffusers consists of separating the physical spaces in which the dissolution and the reaction occur. This approach can be done through a sidestream injection system, which uses either an under positive or negative pressure injector, to which there is a possibility of associating a static mixer, or the static mixer can replace the injector and be used alone. Figure 2D shows a sidestream representation that only uses a venturi injector: thus, a static mixer, such as the one shown in Figure 2E, can either be added after the injector, or replace it. Therefore, this system only provides a stream of ozonated water, which is then directed to another chamber, where the reaction of oxidation and/or disinfection occurs. As a consequence, the sidestream injection lowers the volume necessary for the reaction zone, in addition to having lower maintenance costs and more flexibility, when compared to the conventional bubble diffuser [5].

The negative pressure injection is typically made by flowing water in a pipe and compressing it through a small orifice in order to create a Venturi effect, i.e. creating a

partial vacuum, which attracts the gas into the flowing water. However, depending on certain factors, such as the ozonized gas pressure available, and downstream treatment units, additional pressuring may be necessary, such that a positive injection would be the adequate approach. This sidestream injection system alone provides an efficient transfer of ozone into the water, with values capable of reaching more than 90% [4,5].

On the other hand, the static mixer is able to provide similar or larger values of transfer efficiency when compared to other mixing methods [5,30], whilst having a series of benefits: it requires small space, it is a cheap equipment, no further power input is required besides the pumping, it does not use moving parts, among others advantages. This equipment can be described as a series of identical, motionless inserts, called elements, whose purpose is to modify the fluid flow, redistributing it in the radial and tangential directions [6,7]. Though there are various static mixers available, which can be found in literature [6]; this work will only focus on the NETmix, as it will be henceforth discussed. The different injector and static mixers designs are responsible for the range of values presented in Table 3, where it can be seen that the static mixers have the highest volumetric mass transfer coefficients among the discussed equipment.

Table 3 - Range of values of volumetric mass transfer coefficients for the equipment most used in the dissolution of ozone in water/wastewater plants (adapted from [31,32]*).*

Equipment	**Range of values of volumetric mass transfer coefficient** / s^{-1}
Fine bubble diffuser	0.0001 – 0.1
Packed columns	0.005 – 0.02
Baffled sparged or self-inducing impellers	0.01 – 0.2
Venturi injectors	0.06 – 0.21
Static mixers	0.1 - 10

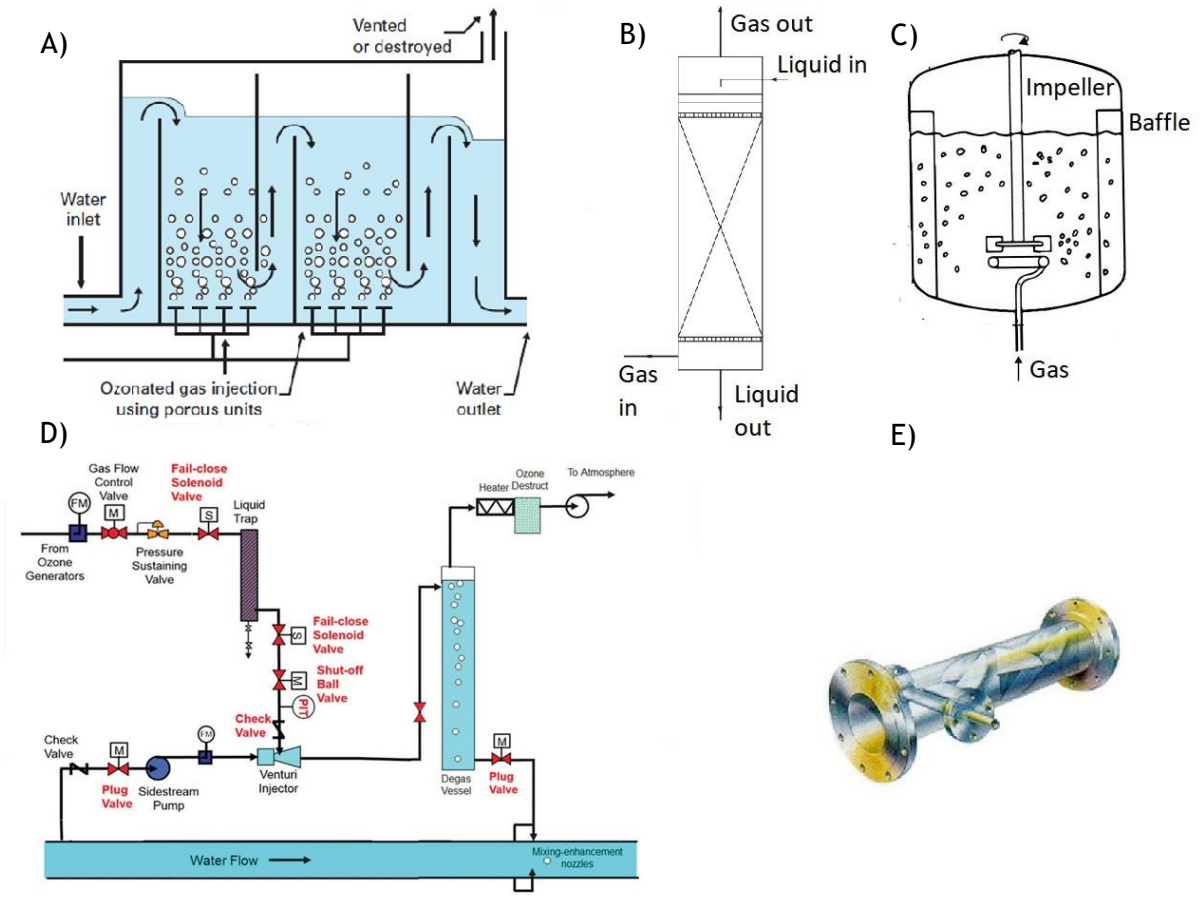

Figure 2 -A) Ozone bubble fine diffuser contactor; B) Packed column; C) Baffled sparged impellers; D) Sidestream configuration using a venturi injector; E) Ozone static mixer from Komax Systems, inc. (adapted from [7,25,29,33,34]*)*

2.3 NETmix

The NETmix is a patented static mixer composed of a network of unit cells: each cell is a chamber connected to two half channel inlets and two half channel outlets, which are oblique in relation to the direction of the flow. As such, the NETmix is a sequential interconnection of these identical unit cells. There are two preferential configurations of the NETmix unit cell, one in which the chambers are spherical and the channels are cylindrical; and other in which the chambers are cylinders with axis normal to the plane that contains the NETmix, and the channels are rectangular prisms [8]. Figure 3 shows a NETmix representation in three-dimensional space, in addition to examples of the unit cells of the two preferential configurations previously described.

A few studies have shown the innovation and efficiency of the NETmix as both a mixer, and a reactor. The macromixing and micromixing capabilities of the static mixer were tested experimentally, and it was demonstrated that the degree of mixing can be controlled, resulting in an environment adequate to complex and fast reactions [9].

Moreover, its energy performance was shown to be competitive with other static mixers available in the market, in which it can operate comparatively at lower pressure drops [10]. These characteristics, along with its versatility and high heat transfer area, have drawn the attention of researchers and industry alike.

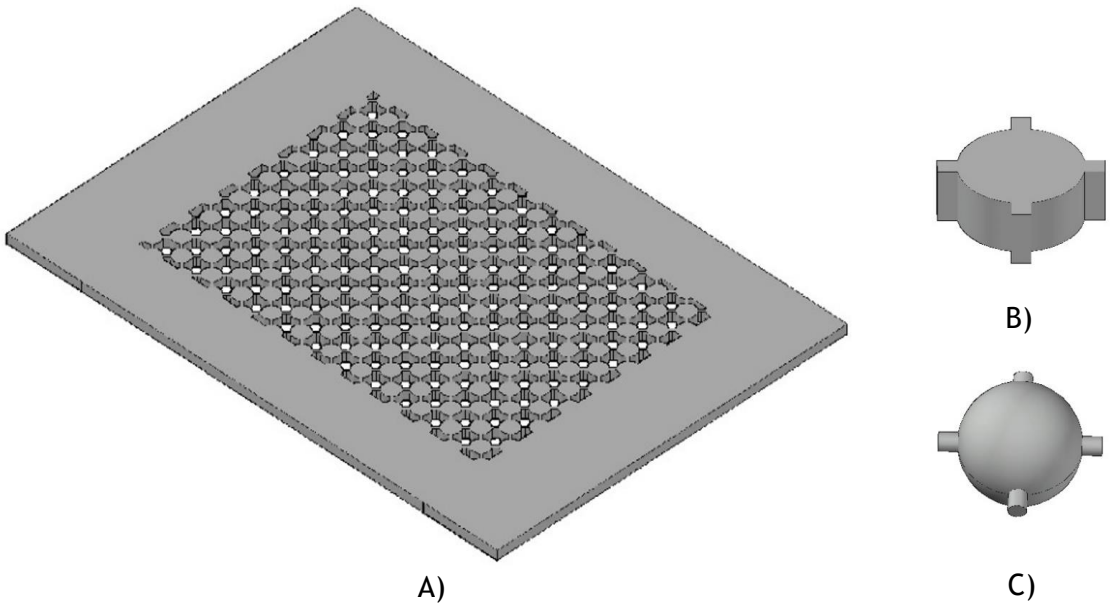

Figure 3 -A) Three-dimensional representation of a NETmix in a plate, in which the unit cells are composed of a cylindrical chamber, and the channels are rectangular prisms; B) Example of a unit cell in which the chamber is a cylinder, and the channel, a rectangular prism; C) Example of a unit cell in which the chamber is a sphere, and the channel is a cylinder.

On the one hand, research has been done to determine innovative applications for the NETmix, in which it has been proven its capability as a photoreactor for homogeneous and heterogeneous reactions: the NETmix was validated for both homogeneous and heterogeneous photo-Fenton treatment of waters containing organic pollutants [35,36]. Additionally, its potential as a photocatalytic reactor was demonstrated for the degradation in liquid phase of contaminants, such as bromate, oxytetracycline, and arsenic [37–39]; as well as in gas phase, such as, volatile organic compounds [40]. On the other hand, the interest of the industry was evidenced by the implementation of a patented process for the production of nanocrystalline hydroxyapatite using the NETmix [41].

However, the majority of the studies have been done either in a liquid phase, or a gas phase, opening the opportunity to the evaluation of the performance of the NETmix as mixer of both gas and liquid, in a multiphase flow, as well as to the investigation of its

application as an alternative apparatus to processes currently applied in industry, and water treatment plants.

2.4 Computational fluid dynamics and its applications

As a third approach to the studies of fluid dynamics, computational fluid dynamics (CFD) is a tool developed to complement the two fundamental and classical approaches: experiment and theory. While CFD will never replace these two, it provides powerful information to aid in their understanding and interpretation. This tool was made possible by the advances in computer technologies, and the creation of numerical algorithms for solving complex equations. As such, CFD is a set of numerical techniques used to solve a mathematical model developed to describe a phenomenon based on the dynamics of the fluid: this model is centred on the equations of conservation of fundamental properties in nature - mass, momentum, and energy. Additionally, the model can be further supplemented in order to provide more information, for example transport equations, which describe the transport and distribution of intensive quantities, such as concentrations; or equations that provide the behaviour of multiple phases in the flow. Consequently, through the resolution of this model, CFD is capable of providing information of the considered phenomenon which is not easily available, such as the pressure, the velocity and the concentration maps associated to the simulated flow [11,42].

The success of CFD is seen through its vast applications in various domains, such as mechanical, naval, civil, environmental, and chemical engineering [11]. Although many of its applications throughout these domains can be cited, there will only be highlights of its uses in chemical engineering, as it is the domain of this work, whereby CFD has been utilised in both academy and industry. As a teaching tool, it provides students a better understanding of the known phenomenon studied by chemical engineering itself, such as the behaviour of flows inside certain reactors [43–45]. Furthermore, it is a tool embraced by researchers to investigate less known phenomena, taking advantage of its ability to give information, not easily obtainable experimentally, about the flow, without perturbing it. For example, it has been successfully used to contribute to understanding the influence of membrane spacers on the mass transfer of a membrane unit; it has become important in the studies of mass transfer phenomena regarding complex reactors; and it has allowed new approaches to the representation of the intricate phenomena of micro-mixing [46–48]. Lastly, the larger value of CFD to the chemical industry lies in the ease to assess the modification of characteristics of equipment in order to investigate its effects in the overall objective of the apparatus, when compared to the traditional modification through

experimentation. Hence, it is useful for designing, optimizing and scaling-up, leading to a more sustainable and flexible approach in the development of more efficient processes. Through a reliable CFD model, different possibilities can be tested, such as it has been done for the optimisation of fine bubble diffuser designs, the construction of membrane distillation designs, or the improvement of sparged impellers [49–51].

The NETmix itself has been the target of a few CFD investigations: in its inception, it was represented by a simple model in order to study the influence of the Reynolds number regarding certain properties of the mixer, in which it was found the critical Reynolds number – a value above which the flow attained an oscillatory behaviour – in accordance with experimental results [6]. Thereafter, a more sophisticated model was introduced, the NETmix Unit Block (NUB), consisting of 5 rows and 3 columns of the mixer, in which the first and third columns are composed of half chambers. It was discussed the plausibility of the NUB to represent a larger NETmix system through a translational periodic boundary in these cut surfaces of the first and third column, and this approach showed itself to be successful in representing the dynamics and pressure drop throughout the mixer [10]. Afterwards, the NUB concept was further analysed by varying the quantity of rows and columns, whereby the optimum configuration was found to be a geometry containing 9 rows and 3 columns, a model named DoubleNUB [52]. Moreover, with the aforementioned rise in interest to use the NETmix as a photoreactor, models have been developed to describe the radiation field over the mixer, by which it was possible to evaluate its efficiency regarding the surface available to illumination sources [53].

Therefore, CFD is an adequate tool to model and simulate the flow inside NETmix mixers. Though most of the studies were performed in a single phase, there are works which show its potential to model a flow involving both liquid and gas [12]. Hence, it is an interesting approach to evaluate the flow of ozone and water inside the NETmix.

3 Materials and Methods

As described in the previous chapter, CFD simulations are centred on the resolution of equations of three conservation quantities - mass, momentum and energy. Thus, three equations can be solved: the mass conservation equation, or continuity equation; the momentum conservation equation; and the energy conservation equation. The flow considered in this work is isothermal, and, as such, the energy conservation equation was not solved.

The multiphase flow can be described by a number of different models, each based on two approaches: Euler-Lagrange and Euler-Euler. The Euler-Lagrange approach is adequate for the simulation of dispersed systems: when one phase is of small size, such as solid or fluid particles, compared to the total system. The phase of small size is called the disperse phase, whereas the other is the continuous phase. Thus, in this approach, the disperse phase is modelled through the definition of particle parcels distributed appropriately to represent the properties of the phase, in which the position and velocities of each parcel is described by ordinary differential equations. Whereas the continuous phase is represented by continuous transport equations. On the other hand, the Euler-Euler approach treats every phase, both disperse and continuous, as a continuum, and, consequently, it utilises continuous transport equations for each phase [42,54].

The Lagrange-Euler approach is not appropriate for the flow of this work, as the gas and the liquid are both occupying considerable volume fractions inside the NETmix: consequently, the Euler-Euler approach was used. The commercial CFD software ANSYS Fluent 18.2 is utilised in this work, and it has three built-in models for multiphase flow simulation: Volume of Fluid (VOF), mixture model, and Eulerian model. Each model is differentiated only in the way that the disperse phase is treated. The VOF uses a single set of momentum equations for the fluids, resulting in only one velocity field shared by all phases; the mixture model solves a set of mixture equations derived from average properties of the phases, producing separate velocity fields for each phase; and the Eulerian model solves a separate set of equations for each phase. In this work, the VOF model was chosen, as it is simpler, yet adequate to track the position of the interface between the gas-liquid flow [54]. Therefore, the equations associated with this model will be hereinafter described.

3.1 Volume of Fluid model

The tracking of the interface between both phases is done through the concept of volume fraction: it is the ratio of the volume of a phase inside a cell and the volume of the cell. In this work, there is only a liquid and a gas phase, and, as such, all equations will be denoted considering only those two terms. The volume fraction of the liquid phase, α_L, and the volume fraction of the gas phase, α_G, in a cell, individually, must be a value between 0 and 1. Additionally, the sum of volume fraction of the gas and the liquid must be 1 in every cell. Therefore, in most cells, the volume fraction of a phase is either 0 or 1, with cells containing values in between where the interface is located: through this information, this method reconstructs the interface [55].

As such, the continuity equation is defined in Equation 2:

$$\frac{\partial \rho}{\partial t} + \nabla \cdot (\rho \vec{v}) = 0 \tag{2}$$

in which $\vec{v}$ is the velocity vector field, and ρ is a volume-fraction-averaged mixture density, calculated by Equation 3:

$$\rho = \alpha_L \, \rho_L + \alpha_G \, \rho_G \tag{3}$$

in which ρ_L and ρ_G are the density for the liquid and gas phases, respectively. Defining the gas phase as the primary phase, the volume fraction of the secondary phase, α_L, is calculated by Equation 4:

$$\frac{\partial}{\partial t}(\alpha_L \rho_L) + \nabla \cdot (\alpha_L \rho_L \vec{v}) = 0 \tag{4}$$

The volume fraction of the primary phase is, then, calculated by the aforementioned restriction, whereby the sum of the volume fractions of both gas and liquid must be equal to one in each cell. As a characteristic of the model, only one momentum equation, shown by Equation 5, is solved, resulting into a single velocity field that is shared by both phases.

$$\frac{\partial}{\partial t}(\rho \vec{v}) + \nabla \cdot (\rho \vec{v} \vec{v}) = -\nabla p + \nabla \cdot [\mu(\nabla \vec{v} + \nabla \vec{v}^T)] + \rho \vec{g} + \vec{F} \tag{5}$$

In which p is the pressure; $\vec{g}$, the gravitational acceleration vector; and μ is the volume-fraction-averaged dynamic viscosity, given by Equation 6:

$$\mu = \alpha_L \, \mu_L + \alpha_G \, \mu_G \tag{6}$$

In which μ_L and μ_G are the dynamic viscosities of the liquid and gas phases, respectively. The source term $\vec{F}$ accounts for external forces which do not originate from pressure, gravity or viscosity. These forces can arise from interactions between the phases, resulting into drag force, lift force or surface tension: in this work, only the surface tension was

considered, as it is indispensable for the simulation of gas bubbles [12]. Thus, the model used to simulate this tension was the Continuum Surface Force (CSF) [56], which consists in expressing the force at the surface of the interface as a volume force F_{vol} through the divergence theorem based on the Laplace equation, then, adding it as the source term $\vec{F}$. Equation 7 shows the considered volume force, adequate for two phase systems:

$$F_{vol} = \sigma \frac{\rho \, \kappa_G \, \nabla \alpha_G}{\frac{1}{2}(\rho_L + \rho_G)} = \sigma \frac{\rho \, \kappa_L \, \nabla \alpha_L}{\frac{1}{2}(\rho_L + \rho_G)} \quad (7)$$

In which σ is the surface tension between the phases; κ_G and κ_L are the curvatures associated with the gas and with the liquid phase side of the interface, respectively. The Continuum Surface Force model computes the curvature through local gradients in the surface normal at the interface, such that the curvature associated to a generic phase *q* side of the interface is calculated by Equation 8:

$$\kappa_q = \nabla \cdot \hat{n} = \frac{\nabla \alpha_q}{|\nabla \alpha_q|} \quad (8)$$

In which $\hat{n}$ is a unit vector normal to the surface. As there are only two phases, by the definition of curvature, $\kappa_G = -\kappa_L$, such that Equation 8 gives $\nabla \alpha_G = -\nabla \alpha_L$.

3.2 Geometry and mesh

A geometry is the spatial domain inside which the CFD model - the set of mathematical equations – is implemented. The NETmix has already been simulated through a validated geometry, the NETmix Unit Block (NUB), and its variations, albeit not yet experimentally validated for a gas-liquid flow [10,52]. The NUB, as previously stated, uses a translational periodic boundary in order to take advantage of the symmetry and quasiperiodicity of the structured network of chambers and channels. Thus, the NUB enables a model simplification which reduces the required time to perform the simulation, without sacrificing the reliability of the model. In this work, the DoubleNUB configuration, shown to be the best NUB configuration to describe the flow inside the NETmix [52], was used. This configuration is shown in Figure 4, along with its characteristic dimensions, as the NETmix is a network generated by the repetition of unit cells constituted by a chamber and four half channels: D_1 is the diameter of the chamber; L, the length of the channel; and d, the width of the channel.

However, one limitation of the NUB is its incapability of providing information regarding the shape of the entrance, as, in the NUB, the entrance is a half channel, whereas in reality the NETmix can have other entrance shapes. Thus, it was proposed a geometry, named the Half Network Geometry (HNG), to represent the multiphase flow inside a

NETmix, shown in Figure 4, which is a sixth of the total area of a real NETmix unit used in this work. A symmetry plane was imposed in order to extend the capability of the model to simulate a third of the static mixer, as the symmetry condition allows the mirroring of the solution in relation to this plane. This approach opens the possibility to evaluate the influence of the shape of the inlet at which the working fluids make their entrance inside the NETmix regarding the bubble formation. Furthermore, this configuration enables to account for a wall effect, from the last column of chambers, which is not assessed with NUB. Figure 4 shows the characteristic dimensions associated with the HNG, whereby D_2 is the diameter of the smaller chamber; and D_{in}, the diameter of the inlet. It is to be noted that the outlets are only half channels. Through both geometries, two 2D meshes were developed with quadrilaterals of element size 62.5×10^{-6} m, resulting in 92 541 element cells for the NUB, and 312 134 for the HNG.

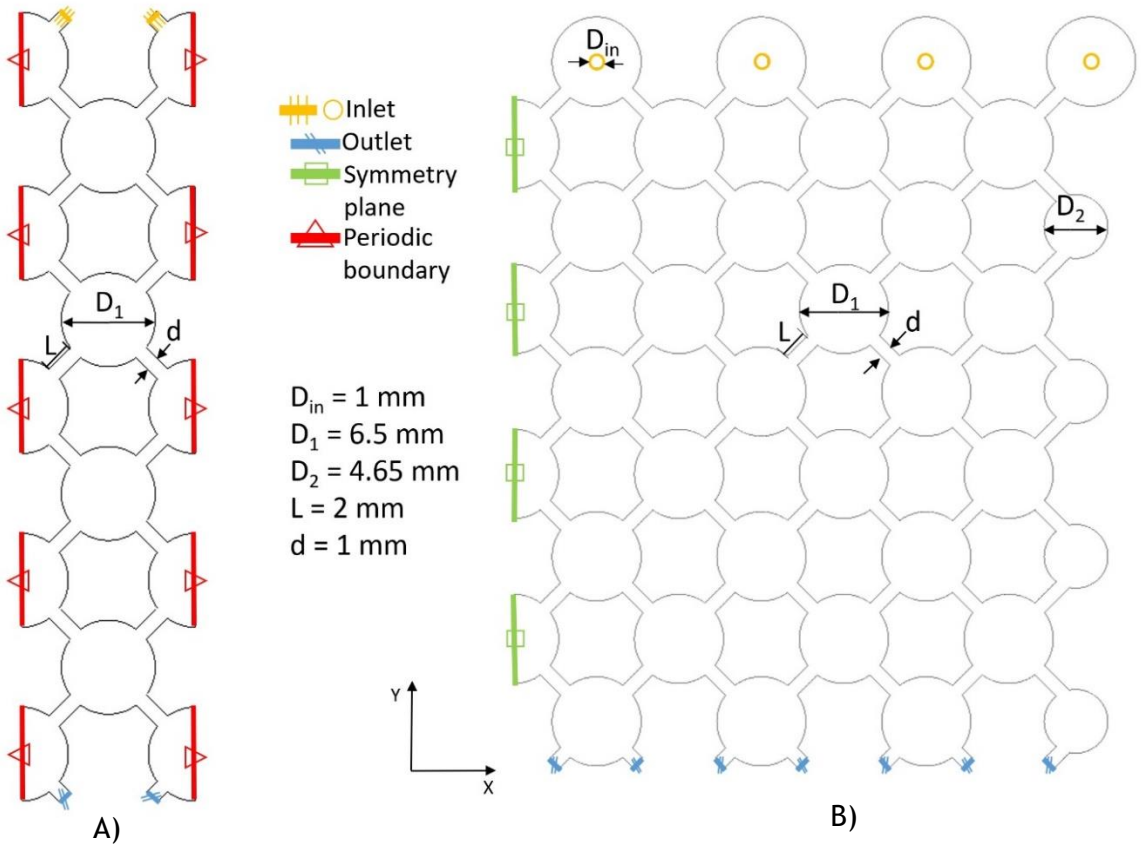

Figure 4 - Geometry, characteristic dimensions and boundary conditions for the A) NETmix Unit Block used in this work; B) Half Network Geometry.

3.3 Boundary and initial conditions

To solve the set of partial differential equations, the CFD tool requires a number of boundary and initial conditions, which are used to delimit the space and time at which the solution is computed. At the inlets, it was determined, through Equation 9, the necessary

mass flowrate $\dot{m}_i$ associated with the volumetric flowrate Q_i used in the lab scale. The mass flowrate was divided between the inlets in such way that the values at each inlet, once summed, would be equal to the total input mass flowrate for the respective phase.

$$\dot{m}_i = \frac{\rho_i \, Q_i}{N_{in,i}} \tag{9}$$

In which the subscript i indicates whether the quantity calculated is for liquid or gas, whereby i is L for liquid and G for gas; and $N_{in,i}$ indicates the number of inlets in which the phase i enters. As it is an important parameter of this work, the calculation of the Reynolds number $\mathrm{Re_i}$ associated with the fluid i was performed by Equation 10:

$$Re_i = \frac{\rho_i \, v_{in,i} \, D_h}{\mu_i} \tag{10}$$

In which $D_h$is the hydraulic diameter and $v_{in,i}$ is the velocity of the fluid i calculated at the first contacting channel, which can be calculated by Equation 11:

$$v_{in,i} = \frac{Q_i}{2 \, N_{in,i} \, A} \tag{11}$$

In which A is the cross-sectional area of the channel. By its geometry, it is the product of its width by its depth. The hydraulic diameter D_h is given by Equation 12:

$$D_h = \frac{4 \, A}{P} = \frac{2 \, w \, d}{w + d} \tag{12}$$

In which P is the wet perimeter. As the depth w in 2D simulations is infinite because there are no viscous stresses in the third dimension, the hydraulic diameter can be simplified into $D_h = 2d$.

Additionally, the outlets utilised an assumption of manometric pressure equal to 0 Pa. For the wall of the geometry, it was established a no-slip condition, whereby the fluid has no velocity when it touches it, except for the wall to the left of the HNG, where it was used a symmetry condition in order to rend faster the calculation procedure. Moreover, the wall adhesion angle was modelled through the computation of the surface normal at the live cell next to the wall by Equation 13:

$$\hat{n} = \hat{n}_w \, cos\theta + \hat{t}_w \, sin\theta \tag{13}$$

In which $\hat{n}_w$ and $\hat{t}_w$ are, respectively, the unit vectors normal and tangential to the wall, and θ is a given contact angle. This result, when combined with the calculations performed by the CSF model to determine the surface normal one cell away from the wall, is capable of computing a curvature with which the surface tension is adjusted in Equation 7. This approach develops a dynamic boundary condition for the wall adhesion phenomenon [56].

For simulations with Reynolds number larger than the critical value of 200, an initial condition was created by the development of a steady state flow field through a simulation whereby shear free walls were defined at the middle of each complete chamber, parallel to the y axis. After a steady state was achieved, the walls at the middle of the chambers were removed, and the desired simulation was performed. If the Reynolds number is less than 200, and for this simulation with shear free walls, the adopted initial conditions were a zero velocity and manometric pressure field, and liquid filled geometry [6,12,57].

3.4 Solution methods

The CFD tool solves the set of differential equations through an approximation by the discretisation of the equations themselves. While there are various methods of discretisation [55], each adequate for the different quantities computed, the chosen ones for the spatial discretisation are presented in Table 4. Furthermore, the method of coupling of pressure and velocity, which represents the coupling of the mass and momentum conservations, was the SIMPLEC scheme. All simulations in this work were performed in ANSYS Fluent 18.2.

Table 4 - Chosen spatial discretisation for the indicated quantities.

Quantity	Discretisation
Gradient	Least squares cell based
Pressure	PRESTO!
Momentum	Third-order MUSCL
Volume fraction	Geo-reconstruct

As the calculations performed were transient, the first order implicit time discretisation was selected. Moreover, the adequate time step size Δt was estimated through the Courant-Friedrichs-Lewy (CFL) condition [58], represented by the Courant number Co, shown in Equation 14:

$$Co = \frac{v_{Max}\,\Delta t}{\Delta x} \tag{14}$$

In which v_{Max} is proportional to the maximum fluid velocity, whether it is from the gas or the liquid, and it was calculated by $v_{Max} = 1.5Max(v_{in,i})$; Δx is the mesh element size, which was 62.5x10^{-6} m. As such, it was determined a time step size that resulted in a Courant number equal to 0.05. The duration of the simulation was based on a proportional value of the passage time τ, calculated by Equation 15:

$$\tau = \frac{A_{geometry}}{\left(N_{in,G}\ v_{in,G} + N_{in,L}\ v_{in,L}\right) d} \quad (15)$$

In which $A_{geometry}$ is the area of the used geometry, approximately 1 183 mm^2 for the HNG, and 335 mm^2 for the NUB. It is to be noted that, in the HNG, the half channel to the rightmost entrance chamber must be counted as two half channels in order to reliably calculate the passage time.

4 Results and discussion

4.1 Preliminary study of flow properties

In addition to the validation of the simulation model, experiments were performed to identify different characteristics of the flow regarding the variation of two parameters: the direction of the flow, and the ratio of the value of gas volumetric flowrate and liquid volumetric flowrate. As the NETmix unit was used vertically, there were two possibilities of flow direction: upwards, whereby both gas and liquid flow against gravity; or downwards, whereby the gas and the liquid flow in the same direction as gravity. In this work, only co-current flow was tested, that is, both fluids flow in the same direction. For simplification, in this chapter, the upwards flow will be called upflow, and the downwards flow, downflow. Hence, for both flow directions, 6 volumetric flow ratios were tested in order to identify the main flow properties that are affected by the variation of the two parameters. Table 5 shows each ratio value tested, along with the corresponding Reynolds number associated with the liquid phase and the gas phase as calculated by Equation 10. It can be seen that the liquid Reynolds number was maintained fixed, corresponding to a volumetric flowrate of 28.8 $L \cdot h^{-1}$, while the gas volumetric flowrate was varied so that the desired ratio could be attained. For this experiment, oxygen was used as the gas phase instead of ozone because it was easier to control the values of flowrate injected in the mixer with the available equipment. This could be done as, with regard to the objective of this work, the difference of properties between both gases can be neglected, when within the same conditions. The liquid phase was composed of water. Additionally, there was no pressurisation of the NETmix, and the experiment was performed at room temperature of around 18 °C.

Table 5 -Values of ratio of gas volumetric flowrate and liquid volumetric flowrate tested in the experiment, along with corresponding Reynolds number for each phase.

	Reynolds number	
Ratio of gas volumetric flowrate and liquid volumetric flowrate	**Liquid phase**	**Gas phase**
0.1	500	3
0.25		8
0.5		16
1		32
2		64
4		128

In all experiments, the injection of the fluids was alternated between the chambers, that is, the rightmost chamber is injected with liquid, and the next chamber to the left, with gas, after which this pattern is repeated until the two chambers at the centre. Additionally, the leftmost chamber is also injected with liquid, and this pattern follows to the right, until the two chambers at the centre, resulting in a symmetry of injection, whereby the symmetry plane is the centre of the NETmix. This injection pattern, illustrated in Figure 5, was chosen so that the simulations performed by the HNG, which contains a symmetry plane, could also be compared to the experimental data. Thus, the experiment consisted of photographing the flow inside the NETmix with the aforementioned conditions at different times: the photographic camera used was a Nikon D34000, with lens Sigma 105 mm F2.8 EX DH. Information about the experimental setup used in this work can be found in Appendix A.

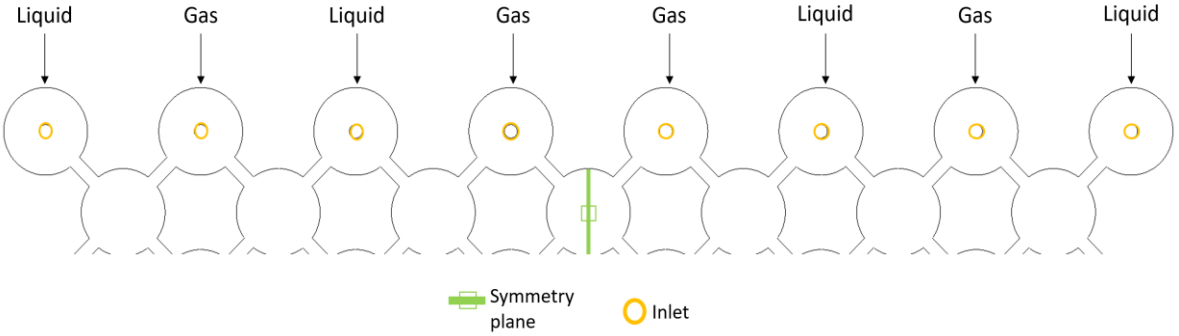

Figure 5 - Pattern of injection of both phases inside the NETmix for all experiments.

The results of the experiment for the upflow direction at ratios 0.1, 0.25 and 0.5 are displayed in Figure 6, whereas Figure 7 shows the ratios 1,2 and 4 for the same direction. The downflow direction is displayed in Figure 8 for ratios 0.1, 0.25 and 0.5, and in Figure 9 for ratios 1, 2 and 4. In each of these figures, the value of the ratio is indicated by the symbol $\frac{G}{L}$, and the gas phase is seen by the contours in contrast.

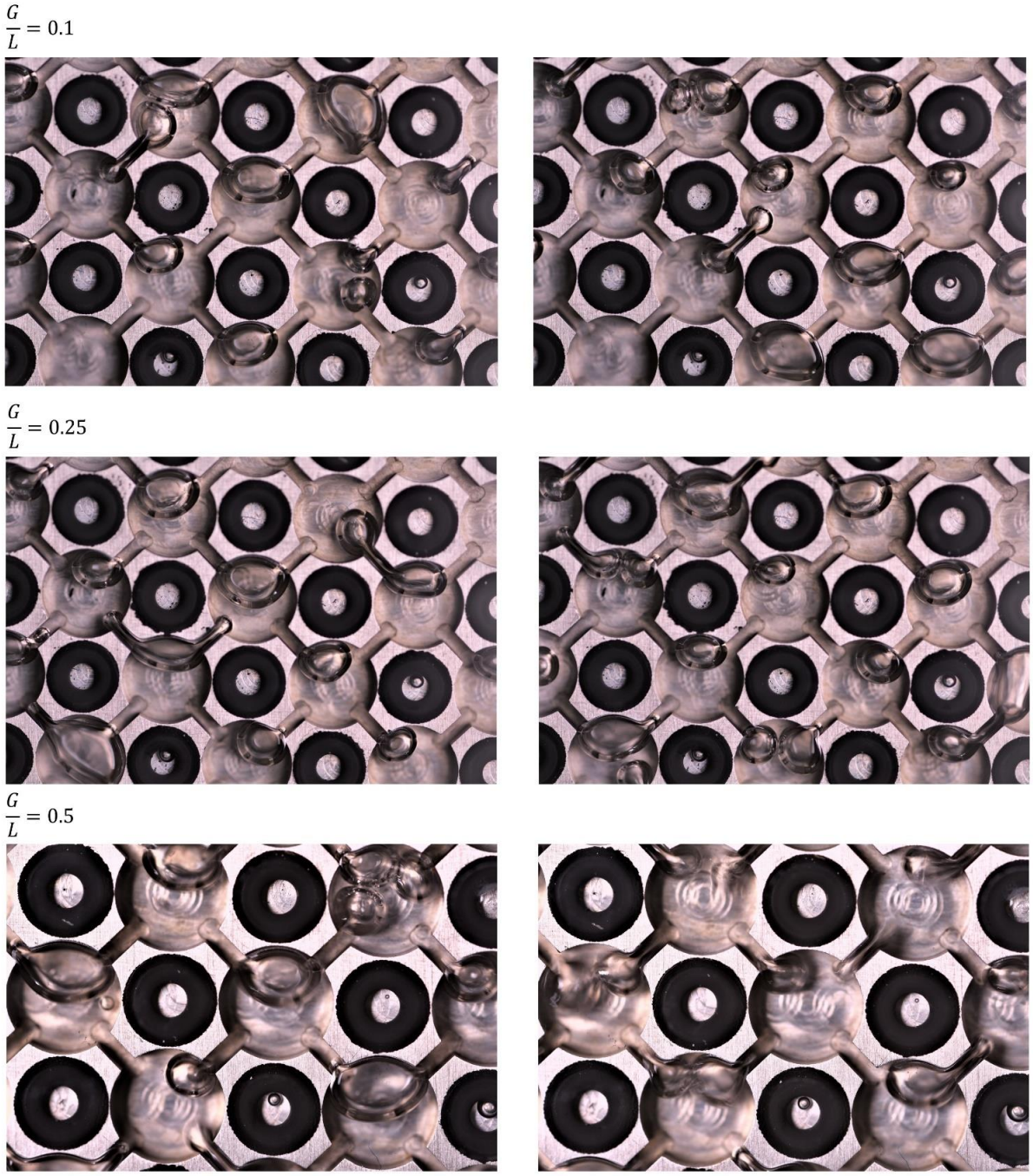

Figure 6 – Flow images for the upflow direction, for the ratio of gas volumetric flowrate and liquid volumetric flowrate ($\frac{G}{L}$) of values 0.1, 0.25 and 0.5.

$\frac{G}{L} = 1$

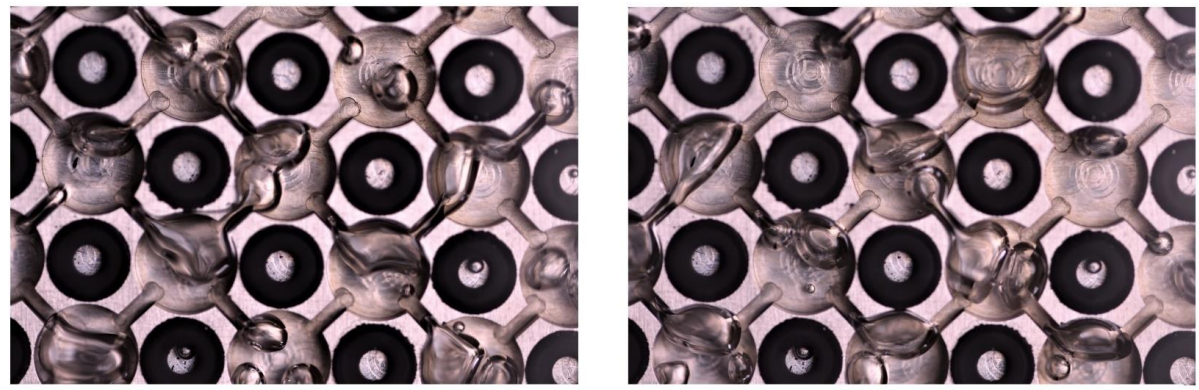

$\frac{G}{L} = 2$

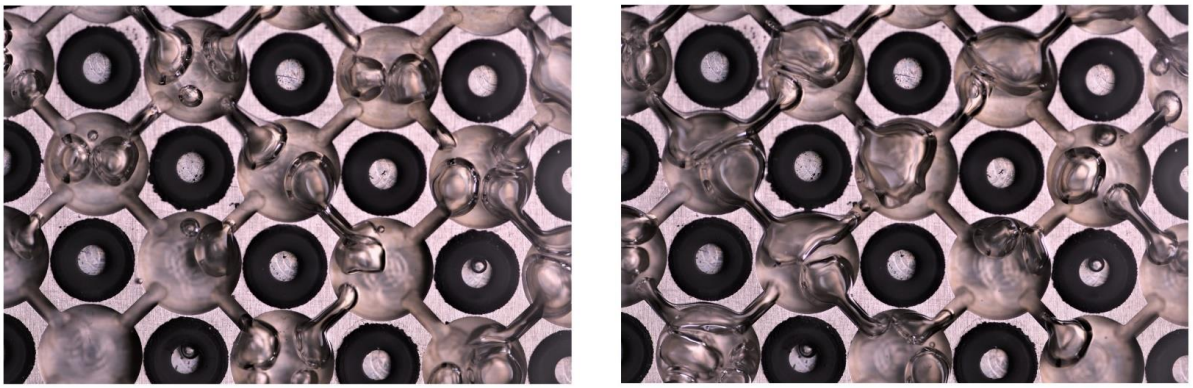

$\frac{G}{L} = 4$

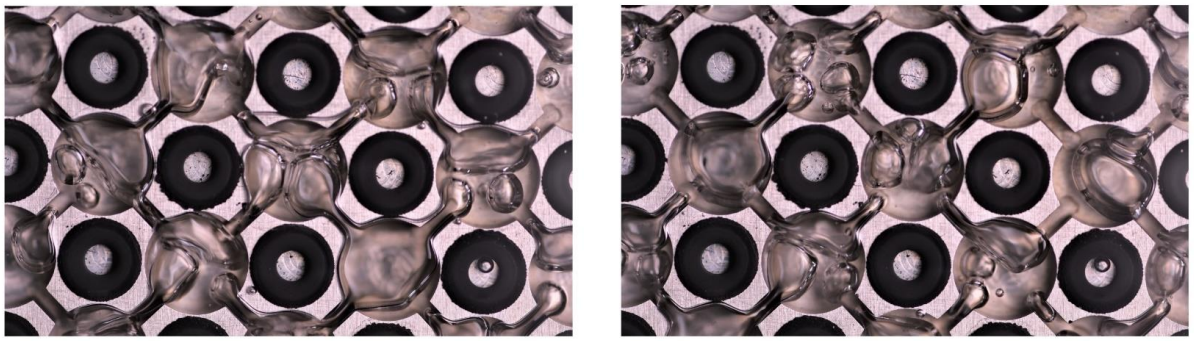

Figure 7 - Flow images for the upflow direction, for the ratio of gas volumetric flowrate and liquid volumetric flowrate ($\frac{G}{L}$) of values 1, 2 and 4.

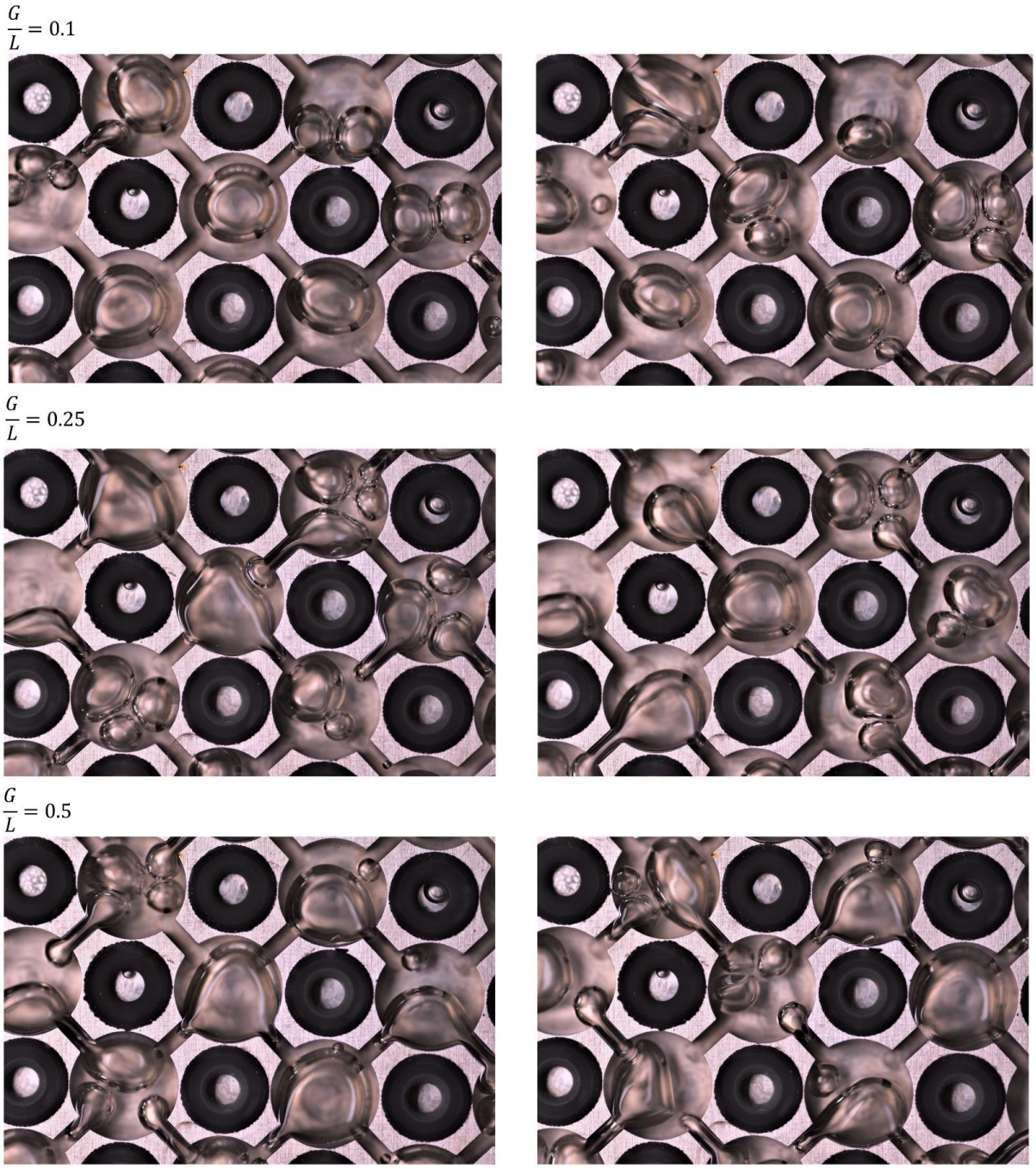

Figure 8 - Flow images for the downflow direction, for the ratio of gas volumetric flowrate and liquid volumetric flowrate ($\frac{G}{L}$) of values 0.1, 0.25 and 0.5.

$\frac{G}{L} = 1$

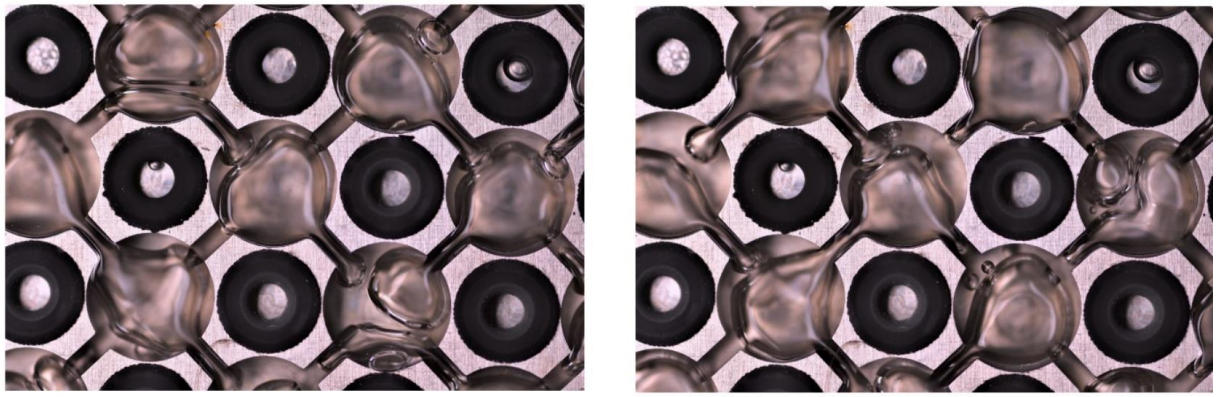

$\frac{G}{L} = 2$

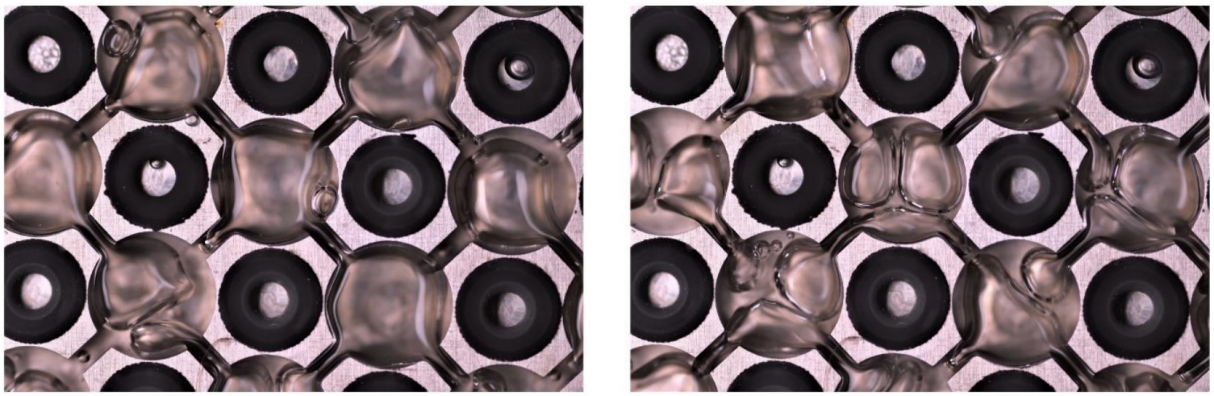

$\frac{G}{L} = 4$

Figure 9 – Flow images for the downflow direction, for the ratio of gas volumetric flowrate and liquid volumetric flowrate ($\frac{G}{L}$) of values 1, 2 and 4.

From the flow images for the upflow direction, it can be observed a characteristic accumulation of the gas phase at the upper part of the chambers of the NETmix for each flowrate ratio value tested, whereas the accumulation of the bubbles tends to be at the centre of the chamber at the downflow direction. Moreover, for upflow, a flow regime transition from bubbly to slug flow is observed. The bubbly flow regime is noted for the smallest gas-liquid ratios - 0.1, 0.25 and 0.5, in which the distribution of bubble sizes is almost uniform, while the slug flow occurs for the highest values of ratio, in which this distribution is non-uniform. Comparatively, the downflow provides an irregular distribution of bubble sizes for all flowrate ratio values tested, whereby it tends to produce larger bubbles than the upflow. The photographs also show that the downflow seems to have more gas inside the NETmix than the upflow, even when the same gas and liquid flowrate is used for both directions, that is, even though the same amount of gas is injected, there seems to have a higher concentration of gas inside the static mixer when the downflow direction is chosen.

Therefore, through the taken photographs, the main flow characteristics for each tested property of the flow (ratio of gas volumetric flowrate and liquid volumetric flowrate, and the flow direction) were identified, of which a more thorough analysis is performed in the next section. As the numerical simulations require a long time to be accomplished, it was chosen only four experiments to be simulated, with which a validation of the numerical model is performed by a comparison of the photographs with the simulation results. Although simulation and experimental results will not be at the same time of the flow, the hydrodynamic characteristics of the flow can be compared. The chosen experiments were the gas-liquid ratios of 0.1 and 1 for each flow direction, thus enabling to capture and to analyse the characteristics of the multiphase flow of gas and liquid inside the NETmix, taking into account the perspective of both experimental and numerical data.

4.2 Analysis of flow properties and simulation validation

As a result of the preliminary study, the chosen parameters to be simulated are summarized in Table 6. Hence, for each selected ratio value, both upflow and downflow were simulated. It is to be noted that Figure 4 displays both geometries at a downflow configuration, in which the upflow consists of swapping the inlets with the outlets for the NUB, and rotating 180º for the HNG. The simulations were done at the exact conditions of the corresponding experiment. It was considered every condition detailed in the previous section, as well as displayed in Table 5.

Table 6 – Selected experiments to be simulated, for which a name is given to the corresponding parameters of the experiment.

Condition	Ratio of gas volumetric flowrate and liquid volumetric flowrate	Flow direction
A	0.1	Upflow
B		Downflow
C	1	Upflow
D		Downflow

Furthermore, the geometry used for the simulation at the conditions displayed in Table 6 was the NUB and Table 7 shows the fluid properties for both oxygen and water considered. As the CSF model enables the consideration of the surface tension between the phases, a value of 73 $mN \cdot m^{-1}$ was utilised. The total simulation time was twice the passage time calculated from Equation 15, the time step size was found to be $8.3x10^{-6}$ s for the four conditions, and, for each simulation, a residual of $1x10^{-5}$ and a maximum of 40 iterations per time step was used as convergence criteria.

Table 7 - Fluid properties used in the simulations of conditions A to D. The decimal places were kept unchanged to indicate the precision used in the simulations.

Fluid	Density / $kg \cdot m^{-3}$	Viscosity / Pa·s
Oxygen	1.2999	$1.919x10^{-5}$
Water	998.2	$1.003x10^{-3}$

4.2.1 Condition A

In this condition, the lower ratio leads to the formation of small bubbles whose size is almost uniformly distributed, resulting in a regime known as bubbly flow. Figure 10 shows the results from the simulation at different indicated times, all of which are compared to

two photographs taken from the experiments performed at the same condition. The passage time for the simulation was calculated to be 1.22 s.

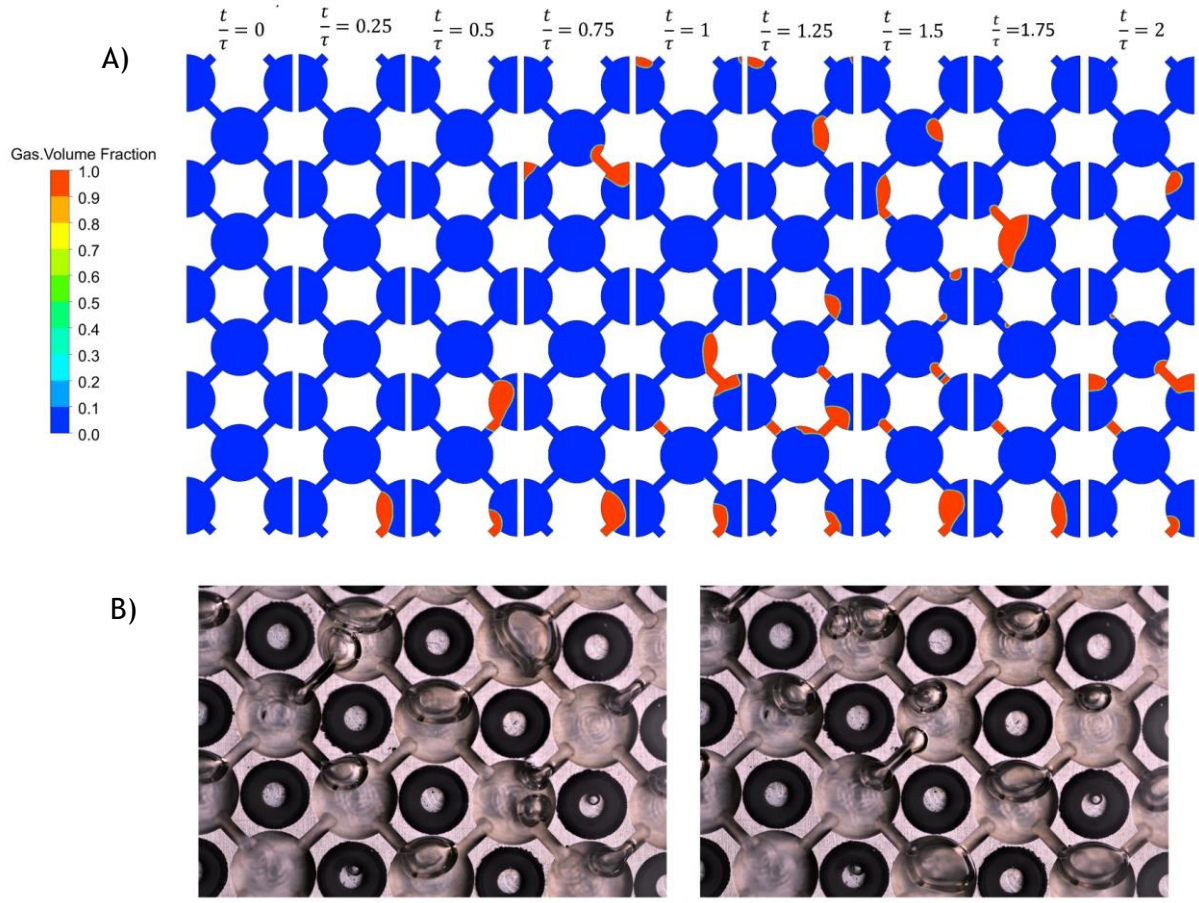

Figure 10 - A) Results, at different indicated times, of the simulation performed at condition A. The gas phase is indicated by the red colour, whereas the blue colour is the liquid phase; B) Two photographs taken from the experiment performed at condition A.

The comparison shows that the shapes of the bubbles are well predicted by the CFD model, which is also successful to represent the stretching of the bubbles when moving from one chamber to the next, as well as the size of the bubbles themselves. A characteristic of the upflow is an accumulation of the gas at the upper part of the chamber, caused by the natural tendency of the gas to flow upwards due to buoyancy. The liquid is able to break the gas into bubbles, in which buoyancy naturally leads these bubbles into the upper part, where there is a possibility of getting trapped by the flow of liquid. Figure 11 shows a highlight of the main trajectory of the water, and it can be seen that the gas can be trapped in the region indicated by the red circle, between the two highlighted paths, while it moves upwards. This phenomenon can lead to an increase in the coalescence of the bubbles, as the gas bubbles coming from the channels below can collide with the gas accumulated in this part of the chamber. This coalescence can reduce

the efficiency of the mixture, as it can create bigger bubbles, reducing the available area of mass transfer between the phases.

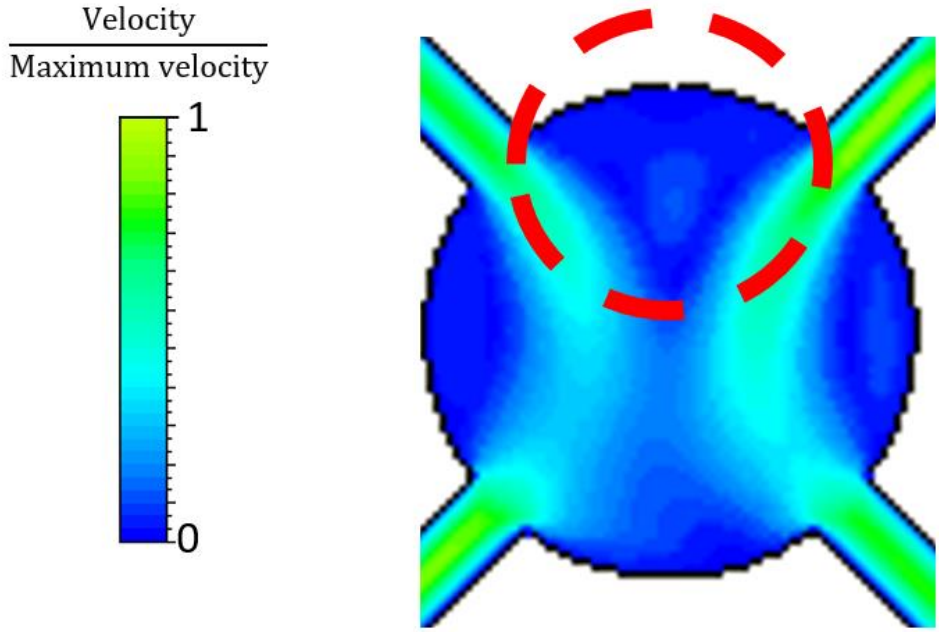

Figure 11 – Velocity contour displaying the main trajectory taken by the liquid, highlighted in green, and the region where the gas bubbles can be trapped, highlighted by the red circle.

As the gas is accumulated, there are bubbles which interact with the surface of the NETmix during a longer period of time, when compared to the bubbles that only travel through the core region of the mixer. Consequently, this longer interaction leads to a full development of bubbles in contact with the surface: this detail is relevant in order to define the considered values of the parameters of the model. To successfully simulate this behaviour, the contact angle between the liquid, the gas, and the solid surface of the NETmix was considered by the model. The contact angle value was experimentally measured, through which the value 88º was implemented, considering the liquid as the secondary phase. Appendix B shows more information about the contact angle measurement utilised in this work.

The CFD model is able to provide a complete picture of the flow, consequently rendering available information about the flow that is difficult to be obtained experimentally. One of this information is the volume fraction of each phase, gas and liquid, inside the overall volume of the NETmix, that is, the ratio of the volume of a phase inside the mixer in relation to the total volume of the mixer. Figure 12 shows the evolution of this quantity during the simulation time, whereby it can be observed that it increases until it is reached a constant behaviour around the value 0.07 for the gas volume fraction, where the

multiphase flow can be considered fully developed. It can be noted that the gas volume fraction is, by definition, the gas hold-up, an important quantity used to describe the multiphase flow in well-known equipment such as a bubble column [59]. In the NETmix, the gas volume fraction is directly related to the mass transfer capabilities of the mixer.

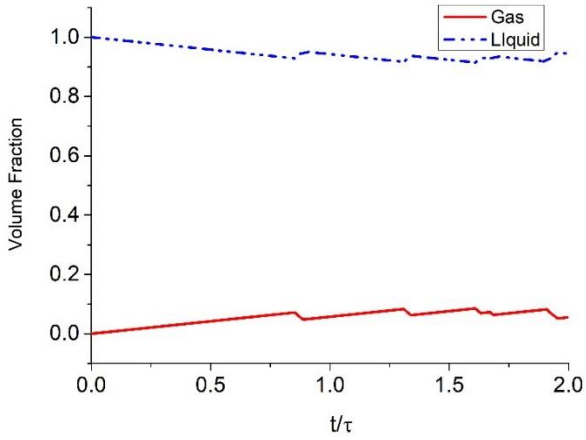

Figure 12 - Evolution of volume fraction of gas and liquid phases for the condition A as a function of time divided by the passage time.

4.2.2 Condition B

When compared with the parameters of condition A, the only difference is the direction of the flow: the same direction as gravity. This is enough to eliminate the accumulation of the gas at the upper part of the chamber, which happened in condition A. As the liquid comes from the channels at the top of the chamber, instead of the bottom, it is able to drag the gas bubbles before they are able to accumulate at the upper part. However, for the downflow, there is a possibility of the bubbles, instead of exiting directly, bouncing at the bottom part of the chamber, which briefly impedes them to move, creating an obstacle to the following bubbles coming from the top: consequently, a brief coalescence situated at the centre of the chamber is possible. The two images in Figure 13 show this flow behaviour.

Moreover, the natural tendency of the gas to move upwards due to buoyancy leads to an additional resistance to its movement downwards, resulting in a slower flow of the gas phase, when compared to condition A, such that the gas is withheld longer inside the NETmix. This result is displayed by the simulations in Figure 13, whereby, at time 2τ, the gas phase still has not reached the end of the mixer, whereas in condition A, the gas reached the outlet by time τ. On the one hand, this longer time in which the gas is held inside the mixer enables a longer gas passage time, favouring the mass transfer of gas into the liquid. On the other hand, this resistance of movement facilitates the aggregation of

the gas phase, which, along with the aforementioned accumulation of the gas at the centre of the chamber, creates larger bubbles, disfavouring the mass transfer, in addition to creating a distribution of bubble sizes less uniform than what was found in condition A. The passage time for this simulation was the same as for condition A, that is 1.22 s.

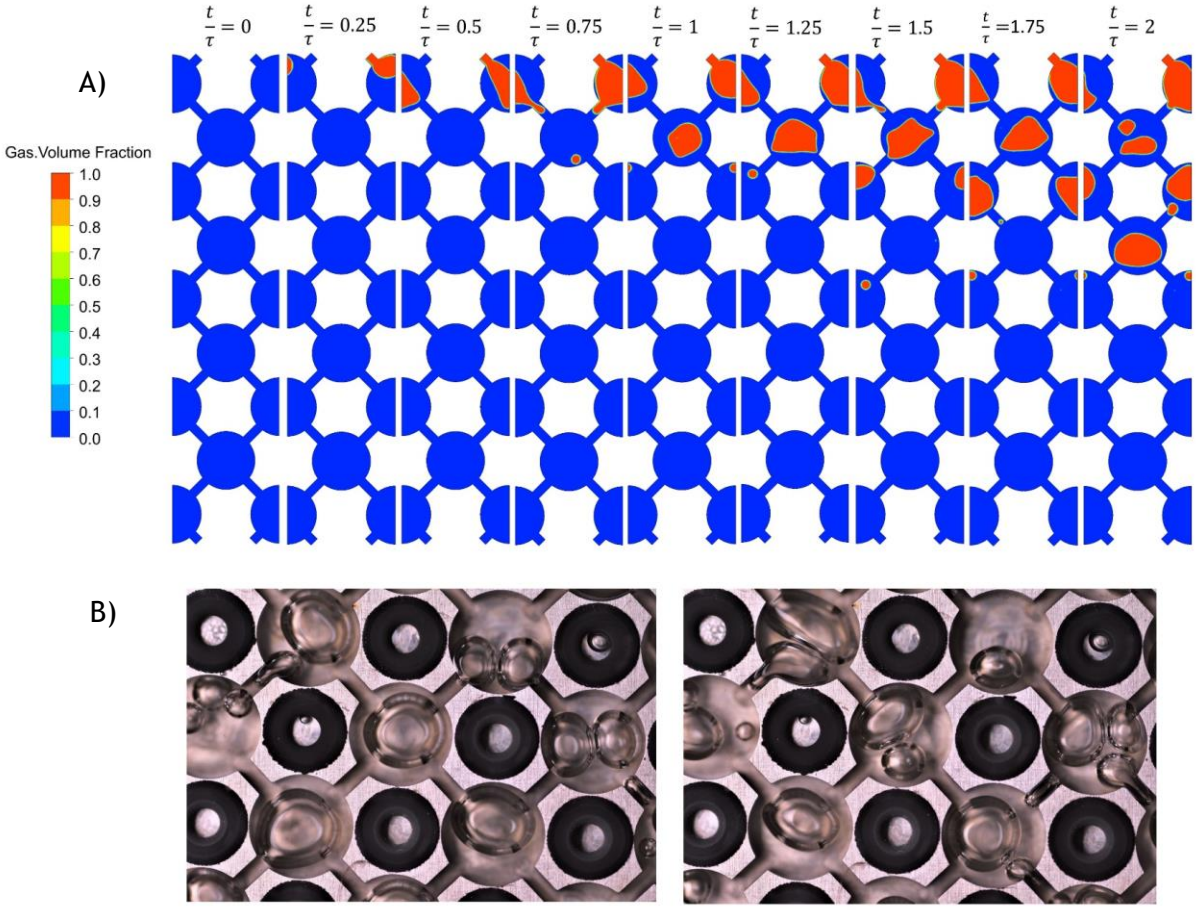

Figure 13 - A) Results, at different indicated times, of the simulation performed at condition B. The gas phase is indicated by the red colour, whereas the blue colour is the liquid phase; B) Two photographs taken from the experiment performed at condition B.

As the gas no longer accumulates at the upper part of the chamber, and, instead, accumulates at the middle, the bubbles interact only briefly with the surface of the mixer. Thus, it was required to adapt the model to account for such brief interaction, such that the contact angle for the downflow simulations was taken as 0º, considering the liquid as the secondary phase, meaning that the gas will not adhere to the surface of the NETmix. Hence, the simulation was capable of capturing the sizes and the shapes of the bubbles, as well as the phenomena related to the movement of the bubble throughout the NETmix, such as the stretching of its shape when it moves between chambers.

An evolution of both gas and liquid volume fractions is shown in Figure 14, in which it is visible that the system has not yet reached a fully developed flow, as the value of gas

volume fraction is still growing. This is consistent with Figure 13, whereby the gas phase is yet to reach the outlet. However, a comparison of value of gas volume fraction can still be made between conditions A and B, in which the gas volume fraction is larger for the condition B, and this condition will be stabilised around an even higher value. This result is a consequence of the gas retention characteristic of the downflow direction, whereby the slower flow of the bubbles leads to a larger accumulation of the gas inside the NETmix, or, in other words, a larger concentration of gas. At 2τ, the value of gas volume fraction for condition B is 0.18, which is more than double the value around which the condition A is developed, 0.07. Such result leads to the conclusion that the downflow direction is more adequate to the dissolution of gas into the liquid inside the NETmix. For the same amount of gas injected into the mixer, the downflow provides a higher gas passage time and a larger concentration of gas, albeit the formed bubbles tend to be of larger diameter. Additionally, this result explains the motive behind the apparent presence of more gas when the photographs for the downflow are compared with the upflow, within the same value of flowrate ratio. Due to the gas retention, the higher concentration of gas feigns the behaviour of the injection of more gas, when the two directions are compared.

Although the results at 2τ have not reached a steady state, they were herein displayed so that they could be directly compared with the results obtained for the other conditions. However, in order to further investigate condition B, the results were extended to reach time 5τ: these results are shown and evaluated in Appendix C.

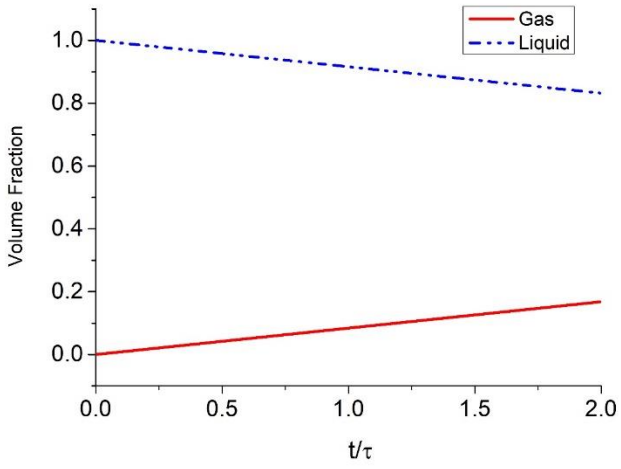

Figure 14 - Evolution of volume fraction of gas and liquid phases for the condition B as a function of time divided by the passage time.

4.2.3 Condition C

By increasing the ratio of gas flowrate and liquid flowrate of condition A by tenfold, the flow regime changes visibly from bubbly flow to slug flow in condition C, which is a flow whose distribution of bubble size is non-uniform, as it is seen in the photographs in Figure 15. The bubbles formed are larger, when compared to the condition A, and the gas visibly occupies larger fractions of the mixer. Moreover, it can be observed that the same phenomenon of gas accumulation at the upper part of the chamber from condition A is still present.

The results from the simulation displayed in Figure 15 show that the model is still capable of predicting the small details of the hydrodynamics of the flow, even though the regime has changed: it is capable of representing from the smallest bubbles to the angular shape of some gas aggregates. It also modelled the bubble formation when the gas moves from one chamber to the next, the size distribution of the bubbles, and the gas accumulation at the upper part of the chamber, for which the same contact angle parameter of condition A was used, 88º. For condition C, the calculated passage time was 0.67 s.

Additionally, the simulation was capable of providing the evolution of volume fraction of both phases, as it is shown in Figure 16. As expected, the injection of more gas leads to an increase of the gas volume fraction, from a value of 0.07 in condition A to 0.27 in condition C, which should increase the mass transfer of the gas into the liquid, although the bubbles that are formed in this condition are larger, and, therefore, provide less surface area to the gas transfer. This suggests that there is a trade-off to be considered, in which the injection of more gas both increases the gas hold-up, and decreases the available specific transfer area per volume of gas, whereby the former favours the mass transfer, whereas the latter is detrimental to this phenomenon. As such, it is expected that there is an optimal value of ratio of gas volumetric flowrate and liquid volumetric flowrate, which maximizes the transfer of gas into the liquid while keeping the injection of gas at the minimum, minimizing the costs associated with it.

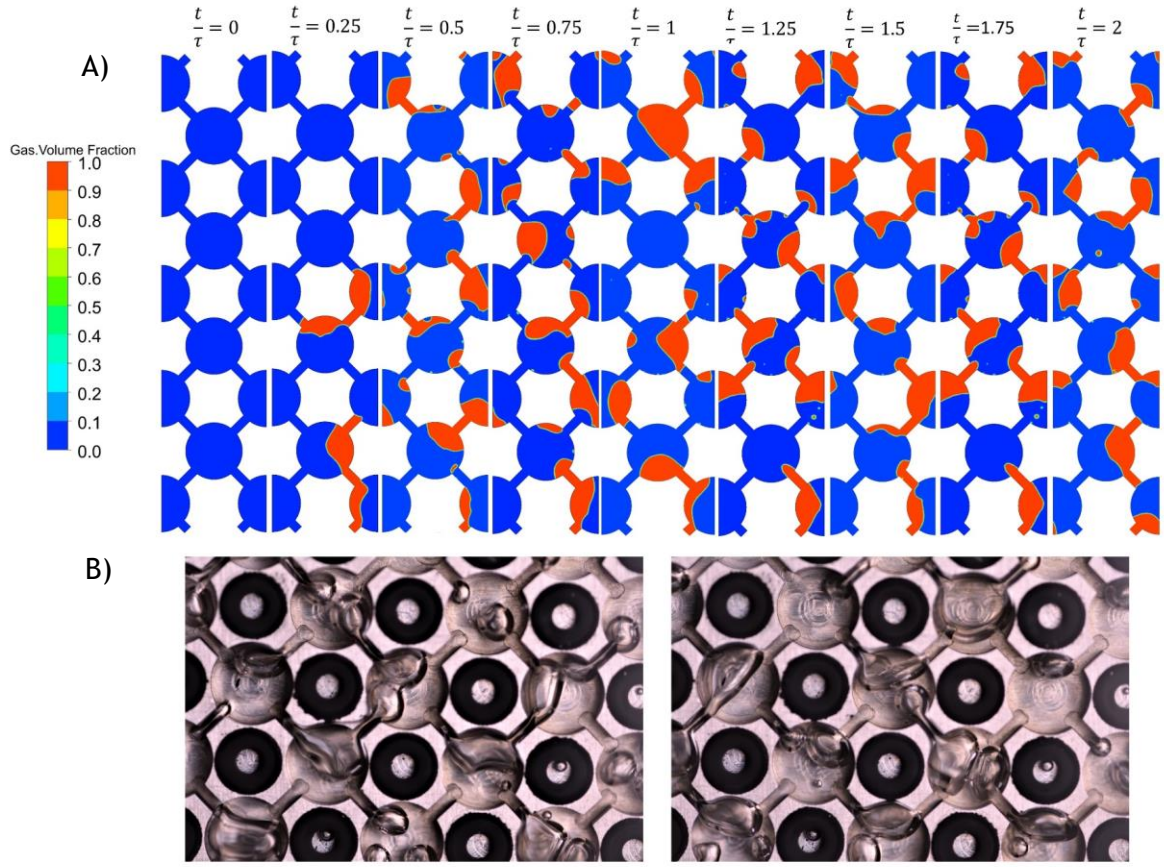

Figure 15 – A) Results, at different indicated times, of the simulation performed at condition C. The gas phase is indicated by the red colour, whereas the blue colour is the liquid phase; B) Two photographs taken from the experiment performed at condition C.

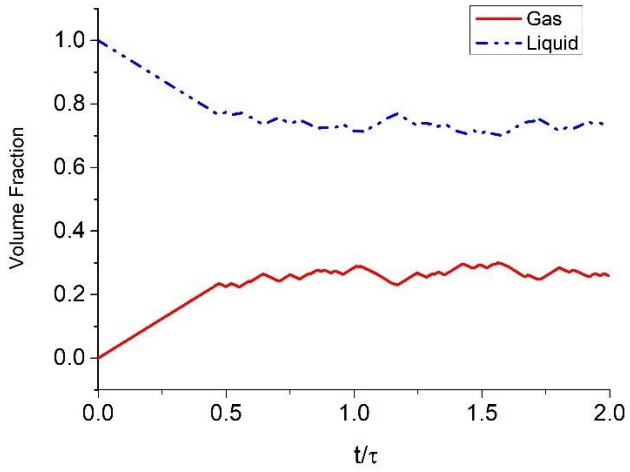

Figure 16 - Evolution of volume fraction of gas and liquid phases for the condition C as a function of time divided by the passage time.

4.2.4 Condition D

Due to the phenomenon of gas accumulation at the centre of the chamber described in condition B, the formed bubbles naturally tended to be larger for the downflow, when compared to the upflow. From condition B to condition D, only the gas flowrate and liquid flowrate ratio was changed, increasing tenfold, which led to the distribution of size of bubbles in condition D averaging at the larger gas aggregates, as it is seen in the photographs of Figure 17: there are, in average, more bubbles capable of filling the entire chamber. The presence of these larger bubbles, when in comparison with condition C, shows that, for the downflow configuration, the gas phase is not broken up by the liquid phase into smaller bubbles as easily as in the upflow configuration. In addition to the gas accumulation at the centre of the chamber phenomenon, the increase in the difficulty to break the gas into small bubbles is also a consequence of the gas retention inside the static mixer, intrinsic to the downflow direction, which raises the concentration of gas.

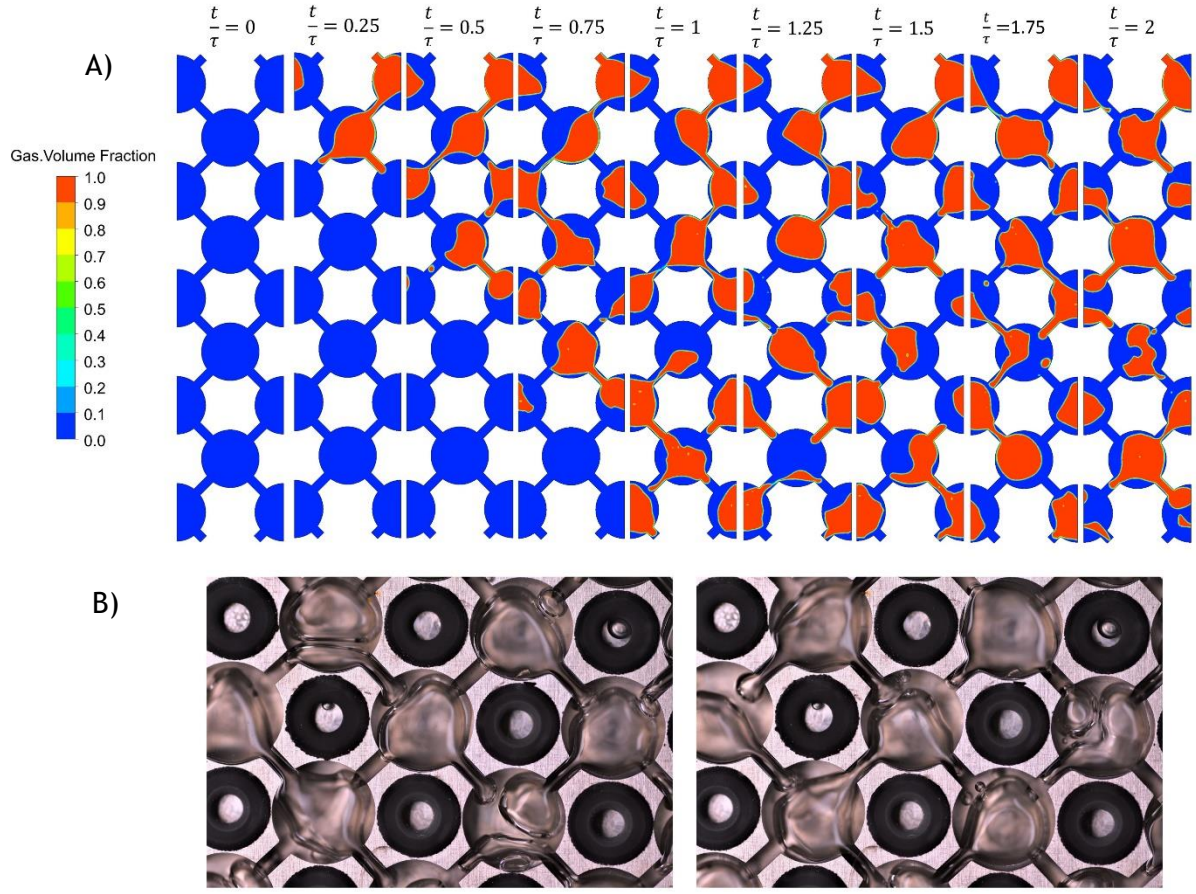

Figure 17 - A) Results, at different indicated times, of the simulation performed at condition D. The gas phase is indicated by the red colour, whereas the blue colour is the liquid phase; B) Two photographs taken from the experiment performed at condition D.

These larger bubbles are well predicted by the simulation, as it can be observed by the results displayed in Figure 17, along with the size distribution of the bubbles, their shape,

as well as the stretching, growth and deformation of the bubbles associated with the movement of the gas throughout the static mixer. Moreover, when comparing the numerical results of all four conditions, it can be observed that the gas requires more time to reach the outlet of the mixer when the downflow direction is used: the condition D required a time of simulation of τ so that the gas could start to leave the mixer, whereas only 0.5τ was needed for condition C. This indicates that globally the downflow direction provides a larger gas passage time, doubling this time when comparing conditions C and D, and more than doubling when comparing A and B. For more precise values in this increase in gas passage time, a more rigorous calculation was performed in Appendix D. As a larger gas passage time favours the mass transfer of gas into liquid, the downflow direction shows itself to provide an advantage over the upflow direction with regard to gas/liquid mixing through the NETmix. The calculated passage time for the condition D was the same as condition C, that is, 0.67 s.

A higher concentration of gas inside the NETmix is observed through the evolution of the volume fraction of gas and liquid phases along the total time simulated, seen in Figure 18. The gas hold-up for the condition D stabilises around the value 0.47, almost double the value around which condition C stabilizes. This further agrees with the conclusion that the downflow configuration favours the mass transfer to the detriment of the upflow configuration, as downwards is the direction by which the injected gas is more efficiently utilised.

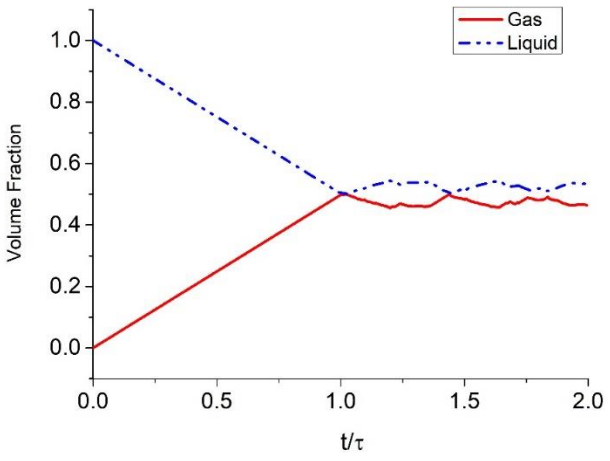

Figure 18 - Evolution of volume fraction of gas and liquid phases for the condition D as a function of time divided by the passage time.

4.3 Analysis of entrance shape influence on the bubble formation

One limitation of the NUB geometry is the incapability of evaluating the shape of the entrance with regard to the bubble formation, as the entrance of the NUB is already a channel. In reality, for the experimental setup used in this work, the entrance was a chamber, in which either phase was injected at the centre of the chamber by a tube of diameter 1 mm positioned perpendicularly to the flow. Hence, the fluids are injected in a direction perpendicular to the ones in which they flow.

On the one hand, the previous results may suggest that there is no influence of the shape of the entrance on the bubble size distribution, and bubble shape, as the entrance shape was not considered, and the simulations still agreed with the experimental data. On the other hand, this conclusion cannot be confirmed until the entrance shape is indeed considered, and its effects, evaluated. Thus, the proposition of the geometry which considers the entrance shape is performed in this work, and its utility in representing the multiphase flow is hereinafter tested.

In order to perform the simulation with this geometry, it was chosen ozone as the gas phase and water as the liquid phase, of which Table 8 shows the fluid properties considered. The Reynolds number of the liquid phase was chosen to be 50, whereas, for the gas phase, it was 9, resulting in a value of ratio of gas volumetric flowrate and liquid volumetric flowrate of 1.5. Due to such low values of Reynolds number, it was chosen the upflow direction, because downflow would result in a divergence error as a consequence of the gas being unable to flow downwards, whereby its buoyancy would prevail over gravity, requiring additional pressurisation of the system, which was undesired. Thus, as seen in conditions A and C, both in upflow direction, for which the contact angle played an important role in the simulations, the contact angle was also accounted at the value 88º, however considering the gas phase as the secondary phase. The surface tension was also considered 73 $mN \cdot m^{-1}$. Furthermore, as the geometry, comparatively to the NUB, is larger, the passage time calculated was 4.72 s, hence, it was chosen to simulate only one passage time, considering the residuals at $1x10^{-4}$, with a maximum number of 40 iterations per time step, and a time step size of $5x10^{-6}$ s to guarantee convergence with each time step.

Table 8 - Fluid properties used in the simulation with the HNG. The decimal places were kept unchanged to indicate the precision used in the simulations.

Fluid	Density / $kg \cdot m^{-3}$	Viscosity / Pa·s
Ozone	1.996	$1.172x10^{-5}$
Water	998.2	$1.003x10^{-3}$

Two photographs taken from the experiment, performed at the same conditions of the simulation, are displayed in Figure 20, whereby it can be seen that the flow is dominated by large bubbles: this is consequence of the lower Reynolds number of the liquid phase, resulting in a low capacity to break the gas into smaller bubbles. Additionally, as expected for the upflow direction, these bubbles are accumulated at the upper part of the chamber.

Furthermore, results from the simulation at four different selected flow times are seen in Figure 20, in which the comparison with the photographs shows that the model with the HNG is capable of representing the multiphase flow and its phenomena, in addition to considering the entrance shape. Consequently, additional information regarding the entrance can be obtained, such as pressure distributions that may indicate the presence of preferential paths of the gas phase during its movement throughout the NETmix. On the other hand, it is visible that the photographs show chambers more filled with gas than what is presented in the simulations: the results shown for the numerical solution are not at the same flow state of the photographs, requiring more time performing the simulation to reach such state. This highlights the biggest disadvantage of using the HNG approach, in which the consideration of additional information for the simulation led to the requirement of more than fourfold the necessary time to conclude the simulations performed with the NUB using the same computer. Therefore, such high computational cost indicates that the HNG needs to be simplified further to be realistically useful, as it is unable to provide results within reasonable simulation time, even if a powerful computer is used.

Though more simulation time would be necessary to fully compare the experiment with the numerical solution, one result can already be obtained through the analysis of the performed simulation alone. When the entrance chamber is partially filled with one phase, such that the phase occupies the entirety of a channel associated with the entrance chamber, the behaviour of this phase, in the entrance, is identical to that obtained by the NUB geometry. Hence, when this occurs, the entrance shape can be removed, as it is done by the NUB approach, and the simulation can be performed independent of the entrance shape. This result is illustrated in Figure 19, whereby it is shown a comparison of the entrance behaviour between the HNG when the entrance chamber is removed, and the NUB, which already does not consider the entrance shape.

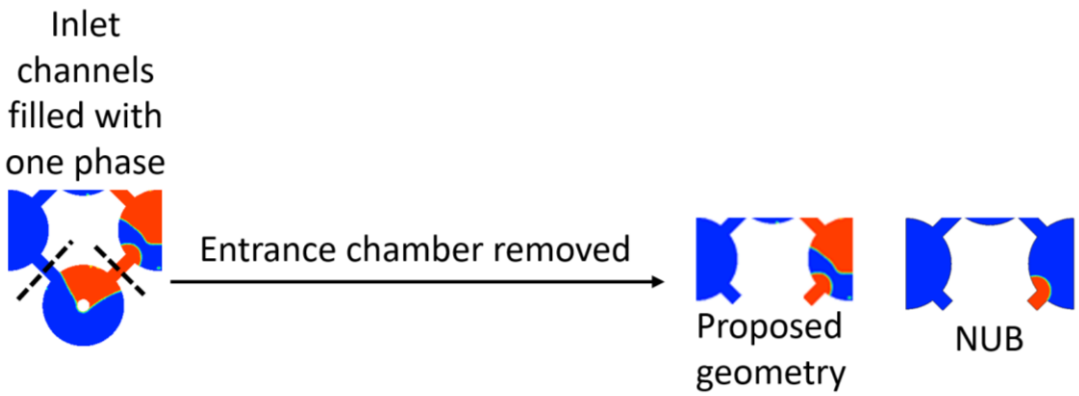

Figure 19 - Comparison of the behaviour of the phases at the inlets between the HNG without the entrance chamber, and the NUB geometry. The picture from the HNG comes from the Figure 20, at time $t = 0.25\tau$; whereas the NUB picture, from Figure 10, at time $t = 2\tau$.

Consequently, the limiting factor of the entrance of the NETmix, regarding the bubble shape formation, is not the shape of the entrance itself, but the dimension of the channel to which the entrance is connected: if the channel is filled with a phase, then the shape of the bubble it produces will not be affected by the shape of the entrance. In other words, the only way that the entrance shape influences the shape of the bubbles is if the phase does not occupy the entire channel, and instead occupies less of it, for example, if the bubble coming from the inlet has a diameter value of less than the width of the channel.

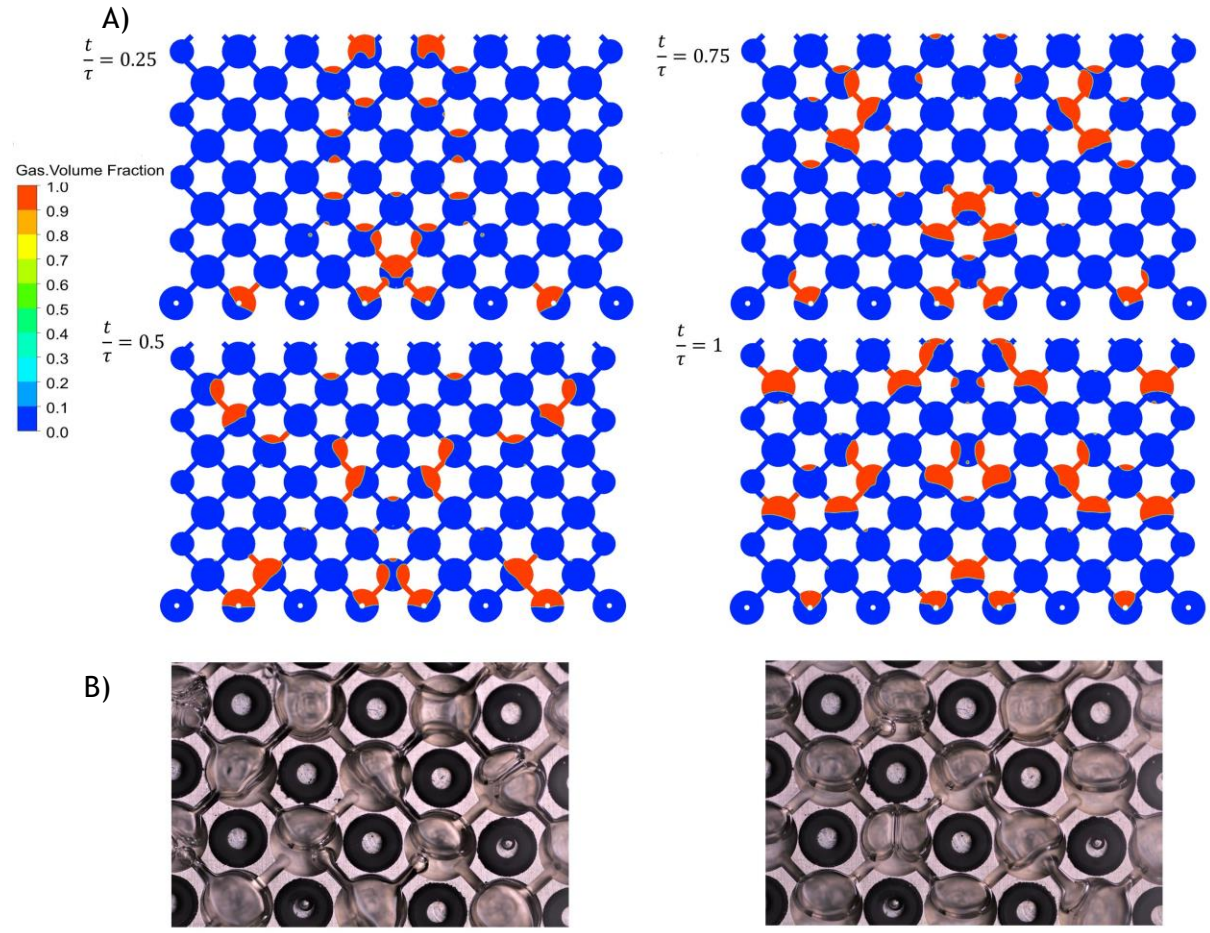

Figure 20 - A) Results, at four different indicated times, of the simulation performed with the HNG. The gas phase is indicated by the red colour, whereas the blue colour is the liquid phase; B) Two photographs taken from the experiment performed at conditions equivalent of the simulation done with the HNG.

5 Conclusion

With the objective of describing the multiphase flow of ozone and water inside the NETmix, this work proposed a CFD model based on the Volume of Fluid approach, which was implemented in two geometries, the NUB as well as a proposed geometry, the HNG. Additionally, experiments were performed to both validate the proposed model and comprehend the main properties and characteristics of the flow of gas and liquid inside the static mixer.

The experiments performed with the variation of the two flow parameters considered (ratio of gas volumetric flowrate and liquid volumetric flowrate, and flow direction) indicated that there is a significant difference between flowing the two phases upwards or downwards. The flow upwards leads to an accumulation of gas at the upper part of the chamber as a consequence of the natural tendency of the gas to move upwards due to buoyancy. In contrast, the gas tends to accumulate at the centre of the chamber for the downwards flow, due to the bubbles which do not exit the chamber directly hitting the bottom part of this chamber, then stopping at the centre of it. Consequently, an obstacle is created for the following bubbles coming from the top, resulting in a collision of bubbles at this region, which generates larger bubbles for the downwards flow, when compared to the upwards flow. Moreover, the variation of the ratio indicated that, for the upwards flow, the regime is transitioned from bubbly flow to slug flow when the ratio is increased, whereas the downwards flow provided a non-uniform distribution of bubble sizes already from the lower values of the ratio tested.

In addition to identifying the main flow properties, the experiments were utilised to comprehend the phenomena associated with the flow and validate the proposed model. Through a comparison of experimental and numerical results, the model was demonstrated to enable an accurate representation of the multiphase flow. This model simulates correctly the phenomena related to all selected ratios and flow directions, as well as predicts the behaviour, shape and size of gas bubbles as they flow throughout the NETmix. Furthermore, the simulations provided additional information about the flow, with which it was possible to conclude that the downwards flow direction is more advantageous to the mass transfer of gas into liquid, as it is associated with a larger gas passage time, as well as a larger concentration of gas inside the mixer. These two results are related to the phenomenon of gas retention intrinsic to this flow direction, consequence of the resistance of the gas to move downwards due to buoyancy. Lastly, the simulation with the HNG showed that the entrance shape has no influence on the

formation of bubble, shape, and size, as long as the gas phase occupies the entirety of the channel associated with the entrance chamber. This means that, if such conditions are met, the decisive factor of bubble formation is the dimension of the channel instead of the entrance chamber. Hence, in this case, the NUB, which does not consider the entrance shape, is a more appropriate geometry for the representation of the multiphase flow, as it provides results in a shorter period of time, comparatively to the HNG.

Therefore, this work proposed a CFD model that can be used to modify operational and geometrical parameters of NETmix units in order to improve its usage to dissolve ozone into water. It is clearly shown the capabilities of the CFD tool in the optimisation of the static mixer with the objective of introducing an alternative mixing method, to be used in ozonation processes in water and wastewater treatment plants, which benefits from the advantages associated with the NETmix to achieve a higher efficiency of ozone utilization.

6 Assessment of the work done

6.1 Objectives achieved

The objectives of this work were successfully accomplished, whereby a multiphase CFD model was developed, and validated with experimental data. This indicates that the model can be used to represent a NETmix unit, as well as to perform further investigations in order to optimise the mixer regarding the dissolution of ozone into water. Furthermore, both experimental and numerical results were utilised to analyse the behaviour of the two-phase flow, through which the main flow phenomena were identified, comprehended, and discussed, leading to conclusions that already aid to determining the best conditions to transfer gas into liquid using the NETmix.

6.2 Final assessment

While the NETmix is the focus of many studies in recent years, only a few were done in a two-phase arrangement, whereby gas and liquid flow, and even fewer were focused on the comprehension of this gas-liquid flow phenomena. As such, this work is a contribution to understanding the potential of this static mixer and is looking to extend the current applications of this technology. Additionally, the developed model enables the possibility to test different designs of the NETmix without building a new physical unit, bringing an advantage into the effort of finding an optimised NETmix unit to dissolve ozone into water.

On the other hand, the numerical results require a lengthy amount of time to be acquired, needing powerful computing machines to provide results within reasonable time. Moreover, the proposed model approach does not consider the concentration of the species, and, therefore, is unable to provide more specific mass transfer information about the flow, such as the volumetric mass transfer coefficient.

Hence, it is proposed as future works the utilisation of the proposed model to investigate different geometric and physical parameters regarding the optimisation of the NETmix to transfer ozone into water. Additionally, whilst the model as proposed in this work does not consider concentrations of species in each phase, it can be extended so that they are considered, which could be interesting to evaluate if such extension is indeed valuable by enabling the determination of mass transfer rates, or if it is reasonable to be neglected.

7 References

[1] B.L. Loeb, Forty Years of Advances in Ozone Technology. A Review of Ozone: Science & Engineering, Ozone Sci. Eng. 40 (2018).

[2] C. Gottschalk, J.A. Libra, A. Saupe, Ozonation of water and waste water: A practical guide to understanding ozone and its application, First Ed., John Wiley & Sons, 2008. https://doi.org/10.1002/9783527613342.

[3] M.S. Lucas, N.M. Reis, G. Li Puma, Intensification of ozonation processes in a novel, compact, multi-orifice oscillatory baffled column, Chem. Eng. J. 296 (2016).

[4] B. Langlais, D.A. Reckhow, D.R. Brink, Ozone in Water Treatment: Application and Engineering, First Ed., CRC Press, 1991.

[5] K.L. Rakness, Ozone in Drinking Water Treatment: Process Design, Operation, and Optimization, First Ed., American Water Works Association, 2005.

[6] P.E.M.S.C. Laranjeira, Ph.D thesis in Chem. Eng., NETMIX Static Mixer - Modelling, CFD Simulation and Experimental Characterisation, Universidade do Porto, 2005.

[7] A. Ghanem, T. Lemenand, D. Della Valle, H. Peerhossaini, Static mixers: Mechanisms, applications, and characterization methods - A review, Chem. Eng. Res. Des. 92 (2014). https://doi.org/10.1016/j.cherd.2013.07.013.

[8] J.C.B. Lopes, P.E.M.S.C. Laranjeira, M.M. Dias, A.. Martins, Network mixer and related mixing process, PCT/IB2005/000647, February 2005. European Patent EP172643 B1, October 2008., 2005.

[9] P.E. Laranjeira, A.A. Martins, M.I. Nunes, J.C.B. Lopes, M.M. Dias, NETmix®, a new type of static mixer: Experimental characterization and model validation, AIChE J. 57 (2011). https://doi.org/10.1002/aic.12316.

[10] C.M. Fonte, M.E. Leblebici, M.M. Dias, J.C.B. Lopes, The NETmix reactor: Pressure drop measurements and 3D CFD modeling, Chem. Eng. Res. Des. 91 (2013) 2250–2258. https://doi.org/10.1016/j.cherd.2013.07.014.

[11] J. Anderson, Computational Fluid Dynamics: The Basics with Applications. 1995, First Ed., McGraw-Hill Education, 1995.

[12] I.S. Fernandes, MSc thesis in Chem. Eng., Two-phase Flow in NETmix Reactors, Universidade do Porto, 2018.

[13] D.M. Desiderio, N.M.M. Nibbering, White's Handbook of Chlorination and Alternative Disinfectants, Fifth Ed., John Wiley & Sons, 2010.

[14] W.H. Glaze, J.W. Kang, D.H. Chapin, The chemistry of water treatment processes involving ozone, hydrogen peroxide and ultraviolet radiation, Ozone Sci. Eng. 9 (1987) 335–352. https://doi.org/10.1080/01919518708552148.

[15] J. Wang, H. Chen, Catalytic ozonation for water and wastewater treatment: Recent advances and perspective, Sci. Total Environ. 704 (2020) 135249. https://doi.org/10.1016/j.scitotenv.2019.135249.

[16] C. von Sonntag, U. von Gunten, Chemistry of Ozone in Water and Wastewater Treatment: From Basic Principles to Applications, First Ed., IWA Publishing, 2012. https://doi.org/10.2166/9781780400839.

[17] K.J. Howe, D.W. Hand, J.C. Crittenden, R.R. Trussell, G. Tchobanoglous, Principles of Water Treatment, First Ed., John Wiley & Sons, 2012.

[18] N. Manivasakam, Treatment of Textile Processing Effluents, First Ed., Chemical Publishing Company Inc., 2013.

[19] D.L. Russell, Practical Wastewater Treatment, First Ed., John Wiley & Sons, 2006. https://doi.org/10.1002/0470067926.

[20] O. Solutions, Ozone solutions, (2021). https://ozonesolutions.com/industries-applications/.

[21] Y. di Chen, X. Duan, X. Zhou, R. Wang, S. Wang, N. qi Ren, S.H. Ho, Advanced oxidation processes for water disinfection: Features, mechanisms and prospects, Chem. Eng. J. 409 (2021) 128207. https://doi.org/10.1016/j.cej.2020.128207.

[22] C. Binnie, M. Kimber, H. Thomas, Basic Water Treatment, Sixth Ed., ICE Publishing, 2018.

[23] P.N. Cheremisinoff, Handbook of Water and Wastewater Treatment Technology, First Ed., CRC Press, 1995. https://doi.org/10.1201/9780203752494.

[24] Juan A. Conesa, Chemical Reactor Design Mathematical Modeling and Applications, First Ed., Wiley-VCH, 2019.

[25] R. Sinnott, G. Towler, Chemical Engineering Design, Sixth Ed., Elsevier, 2020.

[26] C. Schaschke, A Dictionary of Chemical Engineering, First Ed., Oxford University Press, 2014. https://doi.org/10.1093/acref/9780199651450.001.0001.

[27] S.E. Forrester, C.D. Rielly, K.J. Carpenter, Gas-inducing impeller design and performance characteristics, Chem. Eng. Sci. 53 (1998). https://doi.org/10.1016/S0009-2509(97)00352-7.

[28] W.M. Lu, H.Z. Wu, M.Y. Ju, Effects of baffle design on the liquid mixing in an aerated stirred tank with standard Rushton turbine impellers, Chem. Eng. Sci. 52 (1997). https://doi.org/10.1016/S0009-2509(97)88929-4.

[29] S.M. Kresta, A.W. Etchells, D.S. Dickey, V.A. Atiemo-Obeng, Advances in Industrial Mixing - A Companion to the Handbook of Industrial Mixing, John Wiley & Sons, 2016.

[30] R. Munter, Comparison of mass transfer efficiency and energy consumption in static mixers, Ozone Sci. Eng. 32 (2010) 399–407. https://doi.org/10.1080/01919512.2010.517492.

[31] A. Schmitt, J. Mendret, M. Roustan, S. Brosillon, Ozonation using hollow fiber contactor technology and its perspectives for micropollutants removal in water: A review, Sci. Total Environ. 729 (2020). https://doi.org/10.1016/j.scitotenv.2020.138664.

[32] N. Harnby, M.F. Edwards, A.W. Nienow, Mixing in the process industries., First Ed., Butterworths, 1985. https://doi.org/10.1016/b978-0-7506-3760-2.x5020-3.

[33] Suez, Suez's degremont water handbook, (2021). https://www.suezwaterhandbook.com/processes-and-technologies/oxidation-disinfection/oxidation-and-disinfection-using-ozone/selecting-ozonation-reactors.

[34] K.L. Rakness, G. Hunter, J. Lew, B. Mundy, E.C. Wert, Design Considerations for Cost-Effective Ozone Mass Transfer in Sidestream Systems, Ozone Sci. Eng. 40 (2018) 159–172. https://doi.org/10.1080/01919512.2018.1424532.

[35] M.J. Lima, A.M.T. Silva, C.G. Silva, J.L. Faria, J.C.B. Lopes, M.M. Dias, An innovative static mixer photoreactor: Proof of concept, Chem. Eng. J. 287 (2016). https://doi.org/10.1016/j.cej.2015.09.092.

[36] M.J. Lima, C.G. Silva, A.M.T. Silva, J.C.B. Lopes, M.M. Dias, J.L. Faria, Homogeneous and heterogeneous photo-Fenton degradation of antibiotics using an innovative static mixer photoreactor, Chem. Eng. J. 310 (2017). https://doi.org/10.1016/j.cej.2016.04.032.

[37] S.G.S. Santos, L.O. Paulista, T.F.C.V. Silva, M.M. Dias, J.C.B. Lopes, R.A.R.

Boaventura, V.J.P. Vilar, Intensifying heterogeneous TiO 2 photocatalysis for bromate reduction using the NETmix photoreactor, Sci. Total Environ. 664 (2019). https://doi.org/10.1016/j.scitotenv.2019.02.045.

[38] J.C. Espíndola, R.O. Cristóvão, S.G.S. Santos, R.A.R. Boaventura, M.M. Dias, J.C.B. Lopes, V.J.P. Vilar, Intensification of heterogeneous TiO2 photocatalysis using the NETmix mili-photoreactor under microscale illumination for oxytetracycline oxidation, Sci. Total Environ. 681 (2019). https://doi.org/10.1016/j.scitotenv.2019.05.066.

[39] S.G.S. Santos, L.O. Paulista, B.A. Marinho, C. Passalía, M. Flores, M.D. Labas, R.J. Brandi, V.J.P. Vilar, A step forward on NETmix reactor for heterogeneous photocatalysis: Kinetic modeling of As(III) oxidation, Chem. Eng. J. 405 (2021). https://doi.org/10.1016/j.cej.2020.126612.

[40] B.M. da Costa Filho, G. V. Silva, R.A.R. Boaventura, M.M. Dias, J.C.B. Lopes, V.J.P. Vilar, Ozonation and ozone-enhanced photocatalysis for VOC removal from air streams: Process optimization, synergy and mechanism assessment, Sci. Total Environ. 687 (2019). https://doi.org/10.1016/j.scitotenv.2019.05.365.

[41] J.C.B. Lopes, M.M. Dias, V.M.T.M. Silva, P.A.Q.O. Santos, F.J.M. Monteiro, P.J.C. Gomes, A.Y.P. Mateus, Production method for calcium phosphate nano-particles with high purity and their use, PCT/PT2007/000031, 2007.

[42] F. Ullmann, Ullmann's Chemical Engineering and Plant Design, John Wiley & Sons, 2005.

[43] L.M. Madeira, M.A. Alves, A.E. Rodrigues, Teaching nonideal reactors with CFD tools, Chem. Eng. Educ. 38 (2004).

[44] L.M. Madeira, A. Mendes, F.D. Magalhães, Teaching laminar-flow reactors: From experimentation to CFD simulation, Int. J. Eng. Educ. 22 (2006).

[45] A.E. Rodrigues, Residence time distribution (RTD) revisited, Chem. Eng. Sci. 230 (2021). https://doi.org/10.1016/j.ces.2020.116188.

[46] G.A. Fimbres-Weihs, D.E. Wiley, Review of 3D CFD modeling of flow and mass transfer in narrow spacer-filled channels in membrane modules, Chem. Eng. Process. Process Intensif. 49 (2010). https://doi.org/10.1016/j.cep.2010.01.007.

[47] H. Bouras, Y. Haroun, R. Philippe, F. Augier, P. Fongarland, CFD modeling of mass transfer in Gas-Liquid-Solid catalytic reactors, Chem. Eng. Sci. 233 (2021).

https://doi.org/10.1016/j.ces.2020.116378.

[48] Z. Mao, C. Yang, Micro-mixing in chemical reactors: A perspective, Chinese J. Chem. Eng. 25 (2017). https://doi.org/10.1016/j.cjche.2016.09.012.

[49] J. Tu, G.H. Yeoh, C. Liu, Computational fluid dynamics: A practical approach, Third Ed., Butterworh-Heinemann, 2018.

[50] X. Chen, J. Yao, S.C. Jiang, C. Liu, M. Guo, N. Gao, Z. Zhang, An improved CFD modeling approach applied for the simulation of gas–liquid interaction in the ozone contactor along with structure optimization, Chem. Eng. J. 384 (2020) 123322. https://doi.org/10.1016/j.cej.2019.123322.

[51] M.M.A. Shirazi, A. Kargari, A.F. Ismail, T. Matsuura, Computational Fluid Dynamic (CFD) opportunities applied to the membrane distillation process: State-of-the-art and perspectives, Desalination. 377 (2016).

[52] J.P.N. da S. Torres, MSc thesis in Chem. Eng., Orthogonal Decomposition of Turbulence Flows, Universidade do Porto, 2017.

[53] C. Passaliá, M. Flores, S.G.S. Santos, L.O. Paulista, M.D. Labas, V.J.P. Vilar, R.J. Brandi, Radiation modelling in the NETmix photocatalytic reactor: The concept of efficiencies in series, J. Environ. Chem. Eng. 8 (2020).

[54] I. ANSYS, ANSYS Fluent Theory Guide, 2017.

[55] V. V. Ranade, Computational Flow Modeling for Chemical Reactor Engineering, First Ed., Elsevier, 2002.

[56] J.U. Brackbill, D.B. Kothe, C. Zemach, A continuum method for modeling surface tension, J. Comput. Phys. 100 (1992) 335–354. https://doi.org/10.1016/0021-9991(92)90240-Y.

[57] P.J.C. Gomes, MSc thesis in Chem. Eng., The NETmix Reactor Strategies for Optimizing Mixing and Development of New Reactor Designs, Universidade do Porto, 2011.

[58] R. Courant, K. Friedrichs, H. Lewy, On the Partial Difference Equations of Mathematical Physics, IBM J. Res. Dev. 11 (2010).

[59] U.P. Veera, J.B. Joshi, Measurement of gas hold-up profiles by gamma ray tomography: Effect of sparger design and height of dispersion in bubble columns, Chem. Eng. Res. Des. 77 (1999) 303–317.

Appendix A - Experimental setup

A diagram of the experimental setup used in this work is provided in Figure 21. The oxygen was supplied directly from a cylinder, whereby the mass flow controller adjusted the gas flowrate value injected in the NETmix, whereas the water was injected by a gear pump, in which the rotation of the pump was calibrated, previous to the experiment, with the desired liquid flowrate. Moreover, the liquid containing the gas was recirculated into the NETmix, which would not affect the hydrodynamics of the flow and would require less water to perform the experiment. The configuration displayed in Figure 21 is at a downwards direction, in which both fluids are injected at the top: for the upwards direction, the distributors are connected at the bottom of the NETmix. The author would like to thank Mateus Pituco who kindly provided a diagram from which Figure 21 could be adapted.

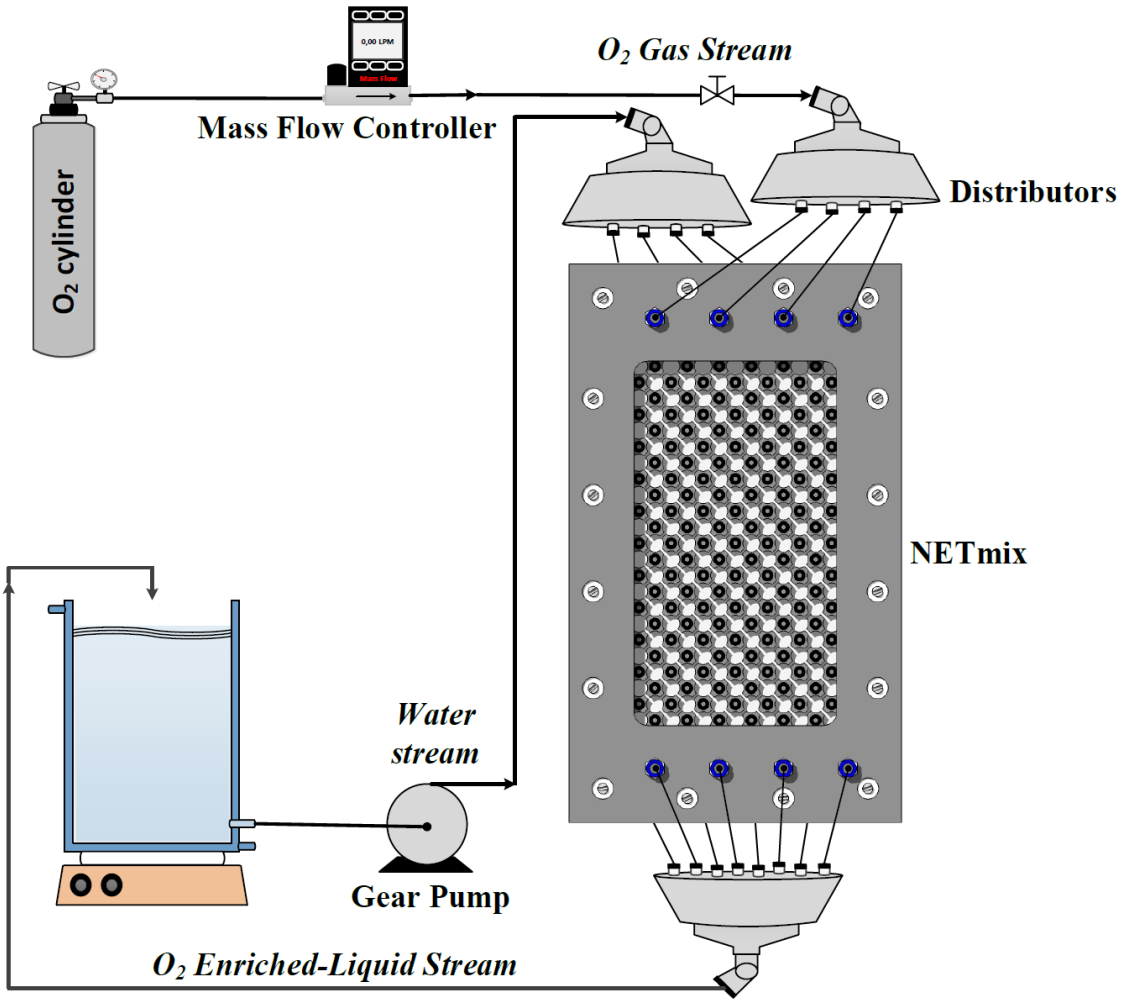

Figure 21 - Diagram with the experimental setup used in this work.

Additionally, a photograph of the NETmix unit, the distributor and the mass flow controller used in this work is displayed in Figure 22.

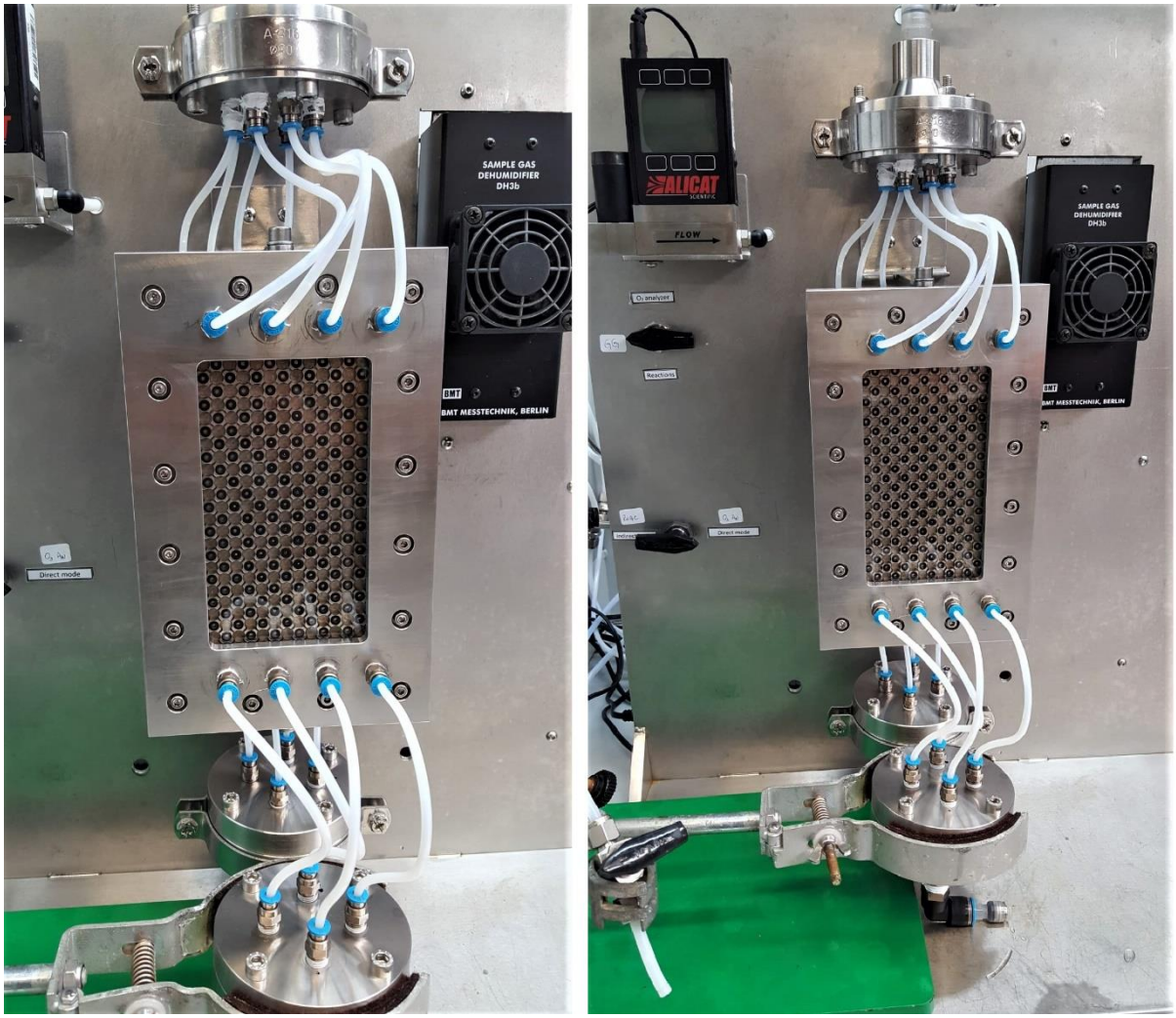

Figure 22 - The NETmix unit, the mass flow controller and the distributors which compose the experimental setup utilised in this work.

Appendix B – Contact angle measurement

As the proposed models included the simulation of the contact angle between the phases, it was necessary to perform the measurement of this quantity. In order to obtain a good approximation, it was used a slab constituted of the same material of the NETmix unit utilised in this work for the experiments – stainless steel 316. Then, this slab was inserted in the equipment *Theta Lite*, whereby a drop of water, with a volume of approximately 5 µL, is dropped onto the surface of the slab, after which the measurement is performed by a camera linked to a software in a computer. The contact angle is measured by the Young-Laplace method, in which a line of reference is adjusted either manually or automatically through the software: the camera allows a recording of the first 10 s of the fall of the drop of water, during which the contact angle is measured multiple times. However, in this work, only the measurements done at the 10 s were considered, in which it was supposed that the system had attained a steady state. Figure 23 shows four measurements performed by the equipment, whereby, in this work, it was used the mean, rounded up, of all the displayed values. As such, the value of contact angle used is of phases air, water and stainless steel 316, which is a good approximation of what is present in the multiphase flow studied.

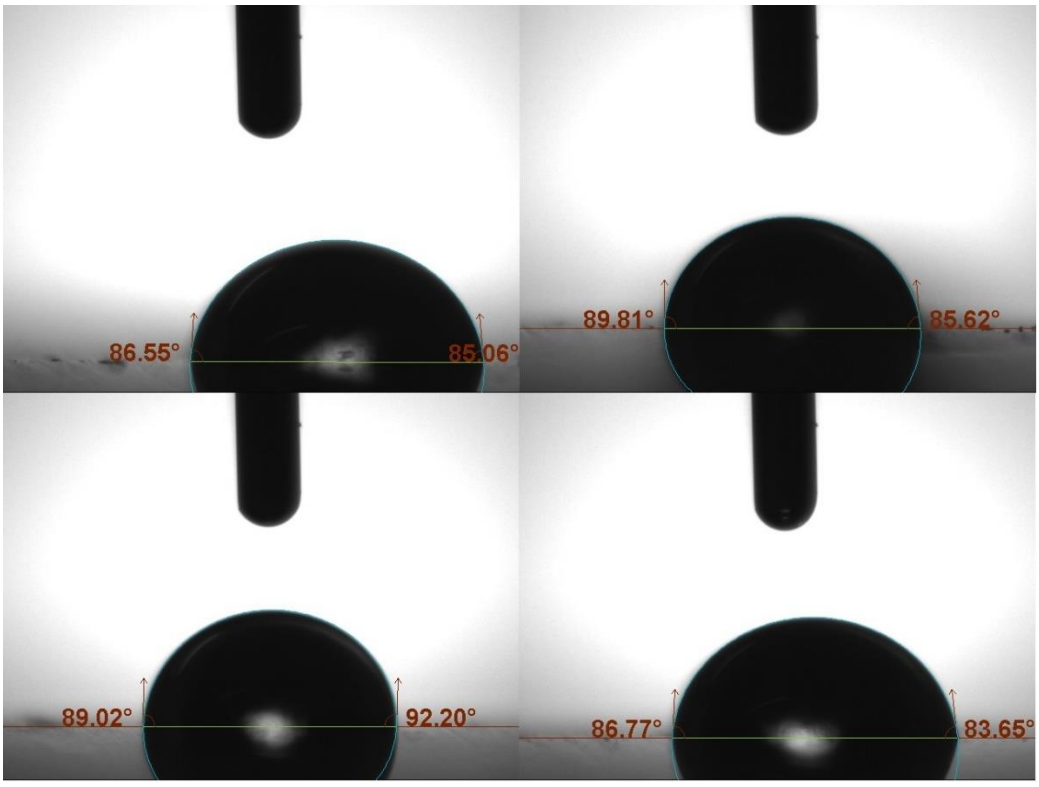

Figure 23 - Picture of each of the four contact angle measurements at 10 s after the drop of water droplet on the surface of the stainless steel 316 slab, containing measurements performed by the software.

Appendix C – Extention of Condition B results

Condition B consisted of selecting the downwards flow direction and the gas/liquid volumetric flowrate ratio value of 0.1. As it was previously discussed in Section 4.2.2, for this condition, the results obtained showed that the gas had not yet reached the outlet at the end of the simulation, which was twice the respective passage time (1.22 s). This displayed the increase in gas passage time when the downwards flow direction was chosen. In order to observe the flow behaviour of condition B in its steady state, it was increased the time during which this condition was simulated to fivefold the respective passage time, for which the results are shown in Figure 24. It can be seen that the gas phase only exits the geometry at around 3τ, which is thrice the necessary time for when the same ratio value is used, but the flow direction is upwards. In other words, the downwards flow direction tripled the gas passage time in the reactor.

Additionally, the volume fraction of both phases as a function of time divided by the passage time was also calculated until fivefold the passage time, as it is shown in Figure 25. From this result, it can be observed that the gas volume fraction averaged around 0.25 when the steady state is reached, which is more than three times that obtained in condition A, 0.07; and almost as high as what was obtained in condition C, 0.27, in which a gas/liquid volumetric flowrate ratio value of 1 was considered. Therefore, the fraction of gas of the condition in which the flow direction was downwards and the least amount of gas was injected was almost as equivalent as when 10 times more gas was injected inside the NETmix when the upwards flow direction was used.

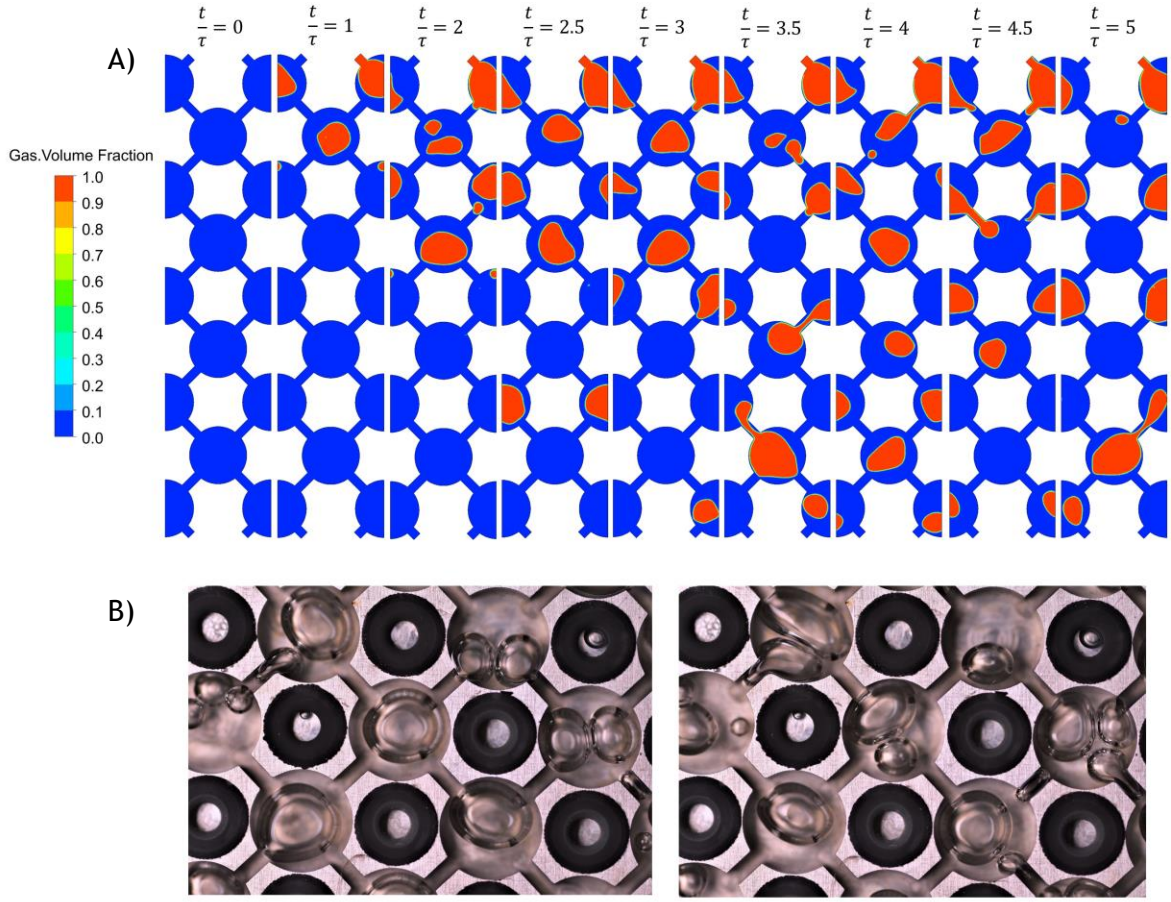

Figure 24 - A) Results, at different indicated times, of the simulation performed at condition B, extended to 5τ. The gas phase is indicated by the red colour, whereas the blue colour is the liquid phase; B) Two photographs taken from the experiment performed at condition B.

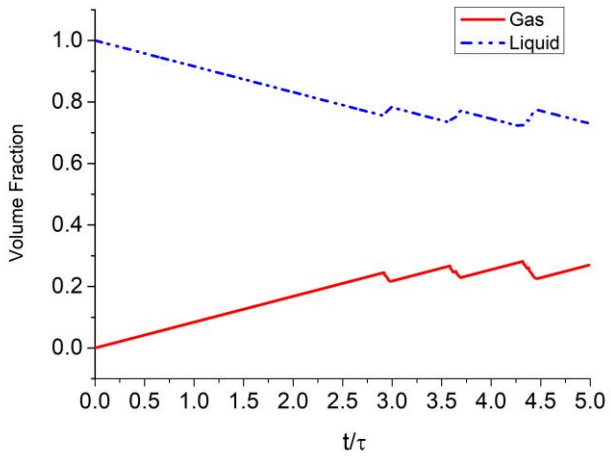

Figure 25 - Evolution of volume fraction of gas and liquid phases for the condition B, extended to 5τ, as a function of time divided by the passage time.

Appendix D - Rigorous calculation of the increase in gas passage time from upwards flow to downwards flow

As seen in Chapter 4.2, and Appendix C, when the gas/liquid flowrate ratio is maintained constant, and the flow direction is changed from upwards to downwards, there is an increase in the gas passage time, which was estimated through the numerical results. It was observed roughly when the gas bubble first reached the outlet of the geometry for each condition, and then these observations were compared, which resulted in the conclusions that for the ratio 0.1, the gas passage time was increased about threefold, and for the ratio 1, it was about twofold. However, these increases can be calculated more precisely, as it will be done hereinafter. The gas passage time τ_G^j associated to a flow direction j – D for downwards and U for upwards – can be calculated by Equation 16:

$$\tau_G^j = \frac{\alpha_G^j \, \mathrm{V_{NETmix}}}{Q_G^j} \tag{16}$$

In which α_G^j is the overall gas volume fraction, as discussed in Section 4.2.1; V_{NETmix} is the volume of the NETmix; and Q_G^j is the gas volumetric flowrate being injected inside the mixer. As the volume of the NETmix is a constant, and the gas volumetric flowrate was invariant with the flow direction, changing only when the ratio value was varied, then, for a given ratio value, the ratio of downwards flow and upwards flow gas passage time τ_G^D/τ_G^U is calculated by Equation 17:

$$\frac{\tau_G^D}{\tau_G^U} = \frac{\dfrac{\alpha_G^D \, \mathrm{V_{NETmix}}}{Q_G^D}}{\dfrac{\alpha_G^U \, \mathrm{V_{NETmix}}}{Q_G^U}} = \frac{\alpha_G^D}{\alpha_G^U} \tag{17}$$

Hence, the averages of the overall gas volume fractions estimated for the steady state of the flow for each condition in Chapter 4.2, summarised in Table 9, can the used to calculate the increase, at the steady state of the flow, in the gas passage time when the flow is changed from upwards to downwards. It can be seen from Table 6 that, from condition A to B, the ratio value was maintained at 0.1, and the flow changed from upwards to downwards; similarly, from condition C to D, the ratio value was maintained at 1, and the flow direction was altered from upwards to downwards. As such, these two pairs, A/B and C/D can be directly compared by Equation 17, resulting in the values displayed in Table 10.

Table 9 - Results obtained for the steady state average value of the overall gas volume fraction for each condition tested in this work.

Condition	Steady state average value of the overall gas volume fraction
A	0.07
B	0.25
C	0.27
D	0.47

Table 10 - Results of the increase in gas passage time when the flow directions is changed from upwards to downwards, for each ratio value tested.

Condition pair	Ratio of gas volumetric flowrate and liquid volumetric flowrate	Ratio of downwards flow and upwards flow gas passage time
A/B	0.1	3.57
C/D	1	1.74

Therefore, it is verified that the downwards flow, when the steady state is reached, more than triples the gas passage time in relation to the upwards flow for the ratio value 0.1, and almost doubles this gas passage time for the ratio value 1, agreeing with the estimations performed in Chapter 4.2 and Appendix C.